

Gibberellins promote polar auxin transport to regulate stem cell fate decisions in cambium

Received: 15 July 2022

Accepted: 30 January 2023

Published online: 30 March 2023

 Check for updates

Riikka Mäkilä^{1,2}, Brecht Wybouw^{1,2}, Ondřej Smetana^{1,2}, Leo Vainio^{1,2}, Anna Solé-Gil^{1,2}, Munan Lyu^{1,2}, Lingling Ye^{1,2}, Xin Wang^{1,2}, Riccardo Siligato^{1,2,4}, Mark K. Jenness³, Angus S. Murphy³ & Ari Pekka Mähönen^{1,2}✉

Vascular cambium contains bifacial stem cells, which produce secondary xylem to one side and secondary phloem to the other. However, how these fate decisions are regulated is unknown. Here we show that the positioning of an auxin signalling maximum within the cambium determines the fate of stem cell daughters. The position is modulated by gibberellin-regulated, PIN1-dependent polar auxin transport. Gibberellin treatment broadens auxin maximum from the xylem side of the cambium towards the phloem. As a result, xylem-side stem cell daughter preferentially differentiates into xylem, while phloem-side daughter retains stem cell identity. Occasionally, this broadening leads to direct specification of both daughters as xylem, and consequently, adjacent phloem-identity cell reverts to being stem cell. Conversely, reduced gibberellin levels favour specification of phloem-side stem cell daughter as phloem. Together, our data provide a mechanism by which gibberellin regulates the ratio of xylem and phloem production.

Vascular cambium is responsible for the lateral (secondary) growth of plant stems and roots. This process is particularly prevalent in tree species but also occurs in non-woody species such as *Arabidopsis thaliana*. The vascular cambium consists of meristematic cells that undergo periclinal cell divisions (that is, cell divisions parallel to the surface of the organ). Cambium cells that leave the meristem ultimately differentiate into parenchymatic or conductive cells, with secondary xylem being produced inwards and secondary phloem outwards^{1–3} (Extended Data Fig. 1a). Recent lineage-tracing studies showed that a subset of cambial cells act as bifacial stem cells, since a single cambial cell is capable of producing both xylem and phloem^{4–6}.

A major regulator of cambium development is the phytohormone auxin^{4,7,8}. Mutations in genes encoding components of auxin signalling, including those associated with perception and polar transport of the hormone, cause defects in cambium development^{4,9},

vascular patterning^{4,9–11}, leaf venation¹², and xylem and phloem formation in planta^{4,13,14}, in tissue culture¹⁵ and during vascular regeneration¹⁶. Recently, we showed that ectopic clones with high levels of auxin signalling force non-xylem cells to differentiate into secondary xylem vessels, while cells adjacent to such clones divide periclinally and gain expression of cambial markers⁴. The ectopic clone thus behaves as an organizer that causes adjacent cells to specify as vascular cambium stem cell-like cells. In agreement with this, an auxin maximum is normally located on the xylem side of the vascular cambium, and stem cell divisions occur adjacent to this maximum⁴. These data raise the question of whether the location of the auxin maximum within the cambium has a role in stem cell fate decisions.

Other phytohormones also influence cambium development alongside auxin⁸. For example, gibberellins (or gibberellic acid, GA) promote secondary xylem production in both *Arabidopsis*¹⁷ and

¹Organismal and Evolutionary Biology Research Programme, Faculty of Biological and Environmental Sciences and Viikki Plant Science Centre, University of Helsinki, Helsinki, Finland. ²Institute of Biotechnology, HiLIFE, University of Helsinki, Helsinki, Finland. ³Department of Plant Science and Landscape Architecture, University of Maryland, College Park, MD, USA. ⁴Present address: European Commission, Joint Research Centre, Geel, Belgium.

✉e-mail: AriPekka.Mahonen@helsinki.fi

poplar^{18–20}. In *Arabidopsis*, this occurs during flowering, when GA levels rise¹⁷. Recently, AUXIN RESPONSE FACTOR 6 (ARF6) and ARF8 have been shown to mediate auxin-dependent xylem production that is downstream of GA signalling²¹. Interactions between auxin and GA also occur in other biological processes. For example, in *Arabidopsis* roots, GA directly promotes abundance of PIN-FORMED (PIN) polar auxin transporters in the root meristem, thus regulating polar auxin transport (PAT)²².

In this Article, we show that GA promotes PIN1-dependent PAT in *Arabidopsis thaliana* roots. This results in an expanded auxin signalling maximum within the root vascular cambium, which forces cambial stem cell daughters to preferentially specify as xylem cells. Our data show how GA influences the position of the auxin maximum in cambium, therefore determining stem cell fate decisions between xylem and phloem.

Results

GA regulates stem cell fate decisions

Previously, GA has been shown to increase xylem formation in *Arabidopsis* hypocotyls during flowering¹⁷. To understand the role of GA on cambial growth dynamics, we analysed GA's effect in *Arabidopsis* roots at a cellular resolution. To reach that goal, we analysed roots during the early stages of secondary growth, when cell division and differentiation dynamics are easier to follow. At these stages, only two types of xylem cell are produced: secondary xylem vessels and xylem parenchyma (Extended Data Fig. 1a). Secondary xylem vessels expand radially and deposit a thick secondary cell wall before fully differentiating into hollow, water-conducting vessels, while xylem parenchyma remain in a seemingly undifferentiated state. As expected, GA treatment in young roots resulted in an increased number of both secondary xylem vessels and xylem parenchyma, and the increase was equal in both cell types (Fig. 1a–c and Extended Data Fig. 1b). In addition, secondary xylem vessel expansion increased as a result of GA treatment (Fig. 1a,d). In contrast to plants treated with GA, a mutant deficient in GA biosynthesis, *ga requiring1* (*ga1* (ref. 23)), had a reduced number of xylem vessels and parenchymatic cells (Fig. 1a–c). Additionally, the xylem vessel area was reduced (Fig. 1a,d). All of these phenotypes were rescued by GA treatment (Fig. 1a–d). Altogether, these data show that GA promotes the production of both xylem vessels and parenchyma during the early stages of secondary growth in roots.

To investigate the mechanism causing the observed changes in xylem cell number, we looked for alterations in the cambium growth dynamics. We used a previously established heat shock-inducible CRE-*lox*-based lineage-tracing system⁴, which allows the production of single-cell clones within a population of dividing cells, including cambium. This enabled us to monitor the cambium growth dynamics over time. Under normal growth conditions, lineages are derived from a single recombination event in one stem cell and span towards both the xylem and phloem side in an almost equal manner (Fig. 1f,i). This indicates that bifacial stem cell divisions normally provide an equal number of new xylem and phloem cells. Under GA-treated conditions, clone cell lineages show an unequal distribution (Fig. 1g,i), with a preference towards the xylem side, while lineages in the *ga1* mutant background preferably span towards the phloem (Fig. 1h,i). We did not observe proliferating sectors exiting the cambium and entering differentiating tissue in any of the conditions (Fig. 1i). These data indicate that GA regulates stem cell fate decisions during cambium proliferation rather than specifically regulating xylem or phloem proliferation.

Dual function of GA on phloem formation

Previous histological studies in hypocotyl²¹ and our lineage-tracing results in root (Fig. 1i) show that GA inhibits phloem production. Next, we tested whether GA affects the production of different phloem cell types. Phloem consists of conductive cells known as sieve elements, together with their companion cells and phloem parenchyma

(Extended Data Fig. 1a). In agreement with the lineage-tracing results, total phloem cell numbers were decreased in GA-treated roots and increased in the *ga1* mutant background (Fig. 1a,e). Next, we used the conductive phloem cell specific marker *ALTERED PHLOEM DEVELOPMENT* (*APL*)²⁴ to determine whether GA affects the production of conductive phloem cells. We observed that the ratio of *APL*-positive cells to total phloem cells was increased after GA treatment and decreased in *ga1* (Fig. 1j,k). Thus, with excess GA, plants produce proportionally more conductive phloem, and with limited GA, they instead produce proportionally more parenchymatic cells. Similar results were observed when quantifying the proportion of sieve elements by safranin staining²⁵ (Extended Data Fig. 1c–e). These results seem counterintuitive compared with the lineage tracing and total phloem number results, where the reverse tendency was observed. We therefore analysed the overall expression pattern of *APL* in more detail. In *ga1*, *APL* expression showed that phloem differentiation is more focused around the primary phloem pole regions and is situated further away from the dividing stem cells than in normal conditions (Extended Data Fig. 1f–h). In contrast, after GA treatment, plants show broader *APL* expression, with phloem differentiation occurring slightly closer to the dividing stem cells (Extended Data Fig. 1f–h). These data indicate that GA inhibits a phloem fate decision by cambial stem cells; however, those few cells that do specify as phloem will preferentially differentiate as conductive phloem.

GA signalling is required in the early xylem domain

Next, we wondered where and how GA affects cambium growth dynamics. First, we aimed to understand which tissue types GA signalling operates in during secondary growth. DELLA proteins act as repressors of GA signalling, and they are rapidly degraded in the presence of GA²⁶. Mutations in one of the *DELLA* genes, *REPRESSOR OF GA* (*RGA*)²⁷, result in increased xylem area²¹ within the hypocotyl and could therefore also have an effect in root secondary growth. Indeed, we found that *pRGA::GFP-RGA*²⁷ showed broad expression in the root cambium, appearing in both the xylem and the phloem. While 3 day GA biosynthesis inhibitor (paclobutrazol, PAC) treatment increased green fluorescent protein (GFP)-*RGA* signal, 24 h GA application led to strong reduction of the signal in all cell types (Extended Data Fig. 2a–f). These results indicate there is active GA signalling occurring during secondary growth in the cambium.

Deletion of 17 amino acids within the DELLA domain of *RGA* (*RGAΔ17*) results in the formation of a dominant, non-degradable version of the protein²⁸. By driving this dominant inhibitor of GA signalling under three different cell type-specific inducible promoters, we investigated where GA signalling is required for its effect on cambium development. Inhibition of GA signalling under the promoter of the early phloem gene *PHLOEM-EARLY-DOF 1* (*PEAR1*)²⁹ did not inhibit xylem production (Fig. 2a,b,e). However, *RGAΔ17* induction under the promoter of the stem cell gene *AINTEGUMENTA* (*ANT*)⁴, and especially under the promoter of the early xylem gene *HOMEBOX GENE 8* (*AtHB8*) (ref. 4) significantly reduced xylem production (Fig. 2a,c–e), with the strongest lines resembling the *ga1* mutant phenotype (Figs. 1a and 2d). These data indicate that GA signalling in the stem cells and in early xylem is required for its role in promoting xylem production. This is also in accordance with measured bioactive GA gradients within poplar stems³⁰, which show a GA maximum in the developing xylem.

GA regulates the width of the auxin response gradient

Earlier clonal activation studies have shown that a local auxin maximum drives xylem formation and promotes cambial cell divisions non-cell autonomously⁴. As GA's effect on xylem proliferation is the strongest in the early xylem cells, where the local auxin signalling maximum is located, we investigated whether GA could regulate the position of this maximum. Using a new red fluorescent protein (RFP)-based version of the auxin response reporter, *DR5v2* (ref. 30) (Methods), we observed

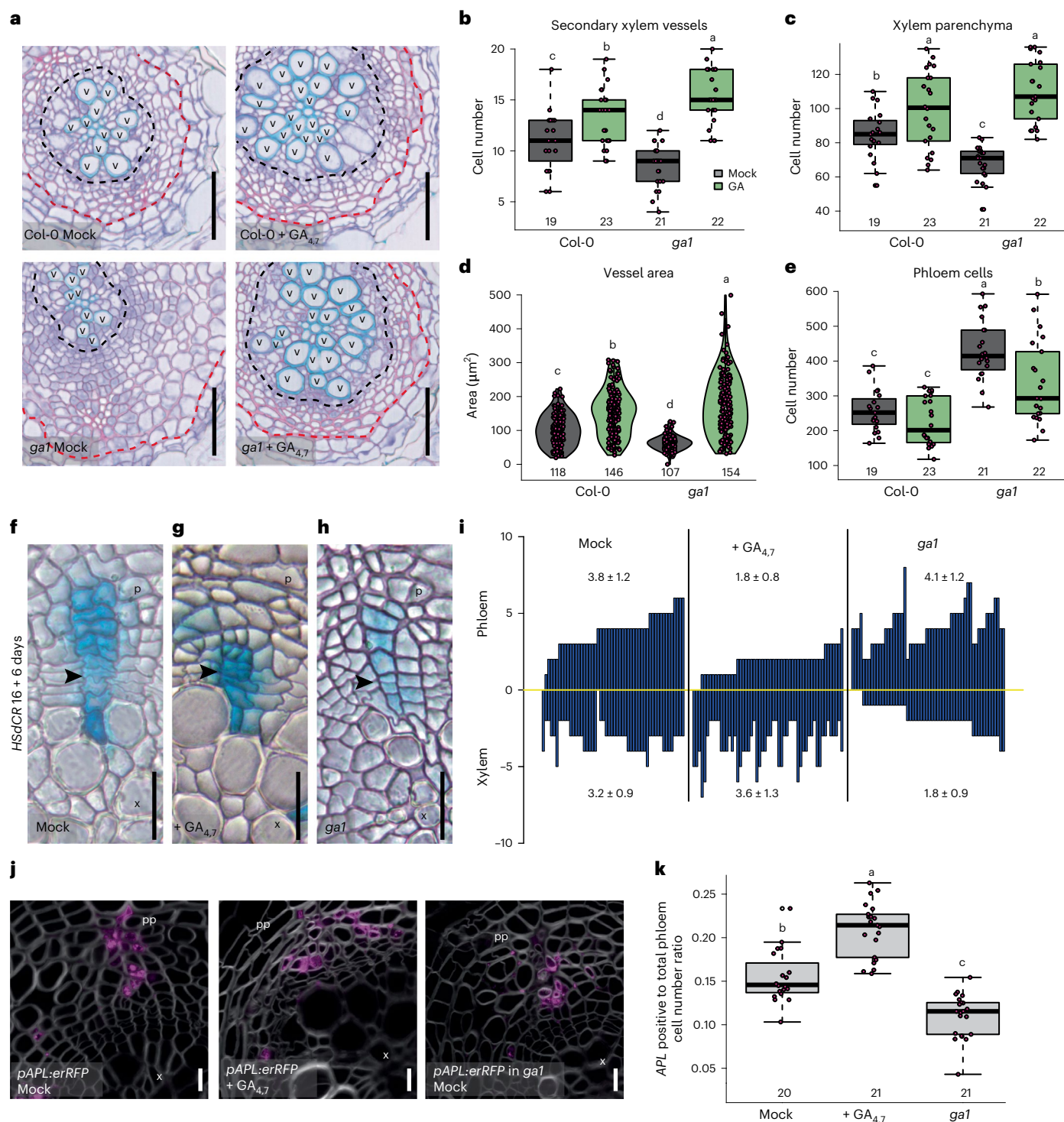


Fig. 1 | GA induces secondary xylem proliferation and vessel expansion.

a, Cross-sections after a 10 day GA treatment in 4-day-old Col-0 and *ga1* roots. Black dotted lines indicate the most recent cell divisions. Red dotted lines mark the border between the phloem and the periderm. **b–e**, Quantifications of secondary vessel (**b**) and xylem parenchyma cell numbers (**c**), individual secondary vessel area (**d**) and total phloem cell number (**e**) in 14-day-old seedlings. **f–h**, Lineage tracing with pHS:Dbx-CRE x 35S::lox-GUS (HsdCR) in active cambium with GUS-stained sectors (blue) originating from a single recombination event. Recombination was induced in 16-day-old seedlings, after which they (Col-0 in **f** and **g** and *ga1* in **h**) were grown for 6 days under mock (**f** and **h**) or GA_{4,7} conditions (**g**). Black arrowheads indicate the most recent cell divisions in the sectors (thinnest cell wall). **i**, GUS sectors (bars) plotted relative to the position of the thinnest cell wall (yellow line) in each sector. Values indicate average number of phloem and xylem cells (± s.d.) within the sectors. **j**, Confocal

cross-sections of *pAPL:erRFP* after an 11 day GA or mock treatment in 4-day-old plants. **k**, The ratio of cells expressing *APL* versus all phloem cells in **j**. In **b**, **c**, **e** and **k**, the boxes in the box-and-whisker plots show the median and interquartile range, and the whiskers show the total range. In the violin plots in **d**, the white dot shows the median and the thick line the interquartile range. The thinner line represents the rest of the distribution. Each side of the line is a kernel density estimation that shows the distribution shape of the data. In **b–e** and **k**, individual data points are plotted as purple dots. Numbers in **b–e** and **k** indicate number of samples. Two-way ANOVA with Tukey's post hoc test in **b–e** and one-way ANOVA with Tukey's post hoc test in **k**. Boxes/bars not sharing a lower-case letter in the plots indicate a significant difference, $P < 0.05$. Scale bars, 50 μm (**a**), 20 μm (**f–h**) and 10 μm (**j**). p, phloem; pp, primary phloem pole; x, xylem; v, secondary xylem vessel. All experiments were repeated three times.

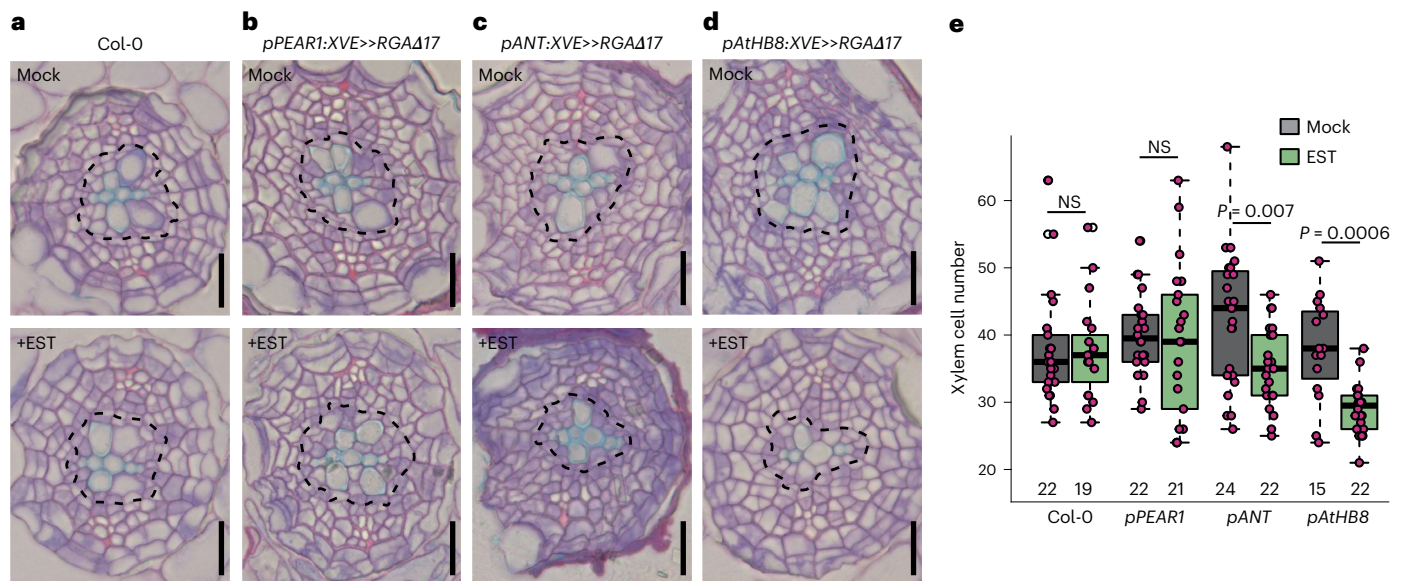


Fig. 2 | GA signalling on the xylem side of the cambium is required to promote secondary xylem formation. a–d. Root cross-sections after a 6 day induction in 4-day-old seedlings of Col-0 (a) or with mutated *RGAΔ17* expressed in the early phloem cell (*pPEAR1:XVE>>RGAΔ17*) (b), the stem cells (*pANT:XVE>>RGAΔ17*) (c) or the early xylem (*pAtHB8:XVE>>RGAΔ17*) (d). Black dotted lines indicate the most recent divisions. **e.** Quantification of the total xylem cell number (cells within the

most recent cell divisions) in a–d. Scale bars, 20 μm (a–d). Significant differences based on a two-tailed Wilcoxon test are indicated. NS, not significant. Numbers in e indicate number of samples. The boxes in the box-and-whisker plots show the median and the interquartile range, and the whiskers show the total range. Individual data points are plotted as purple dots. p, phloem; x, xylem. All experiments were repeated three times.

expression on the xylem side of cambium (Fig. 3a and Extended Data Fig. 3a,f), matching with the cells showing the highest levels of auxin signalling in secondary tissues⁴. Recent stem cell divisions are identifiable by the appearance of thin cell walls within the cambium (arrowheads in Fig. 3a). We marked the phloem-side stem cell daughter as 1 and the xylem-side daughter as –1 (Fig. 3a). In wild-type (WT) plants, *DR5v2* expression often reaches the xylem-side stem cell daughter (–1) and even reached the cell in position –2, but it was rarely seen in the phloem-side daughter (1). In *ga1*, a smaller proportion of stem cell daughters showed *DR5v2* expression (expression in positions 1 or –1 was seen in 29% of *ga1* roots and 48% of control (Col-0) roots; Fig. 3a,b,d and Extended Data Fig. 3a,b). A 24 h GA treatment was not sufficient to cause changes in *DR5v2* expression (Extended Data Fig. 3c–g). However, after 48 h, a higher proportion of the stem cell daughters expressed *DR5v2* than in mock controls (57% in positions –1 and 1 in *ga1* and 83% in Col-0) (Fig. 3a–c). Altogether, these GA manipulation studies show that GA regulates the position of the auxin signalling maximum within cambium.

Since auxin drives xylem vessel formation⁴, this GA-induced broadened auxin response gradient could explain how GA promotes vessel production (Fig. 1a,b). To test this, we investigated whether auxin signalling is required for the effect of GA on xylem production in the root cambium. Previously, we have shown that auxin signalling in the *Arabidopsis* root cambium acts primarily via MONOPTEROS (MP/ARF5), ARF7 and ARF19 (ref. 4). We therefore treated two different allelic *arf7,19* mutant combinations and the conditional triple mutant *amiMP* (inducible artificial microRNA against *MP* in *arf7,19* (ref. 4); Methods) with GA. No significant changes in the number of secondary xylem vessels were observed in any of the mutant combinations following GA treatment (Fig. 3f,g), indicating that GA's effect on xylem production requires ARF5/ARF7/ARF19-mediated auxin signalling.

The HOMEODOMAIN LEUCINE ZIPPER IIIs (HD-ZIP IIIs) act downstream of auxin signalling^{31,32} to promote xylem identity in the root cambium⁴. A representative member of the family, *AtHB8*, is expressed specifically in the early xylem cells⁴. Since *ga1* has a narrow auxin signalling maximum (Fig. 3b,d), *AtHB8* expression is also reduced in the *ga1* mutant, as shown by quantitative real-time polymerase chain

reaction (qRT-PCR) analysis (Fig. 3e). Inducible overexpression of *mir165a*, which targets the messenger RNAs of all five HD-ZIP IIIs for degradation³³, leads to the inhibition of secondary xylem formation in the root cambium⁴. GA was unable to rescue this phenotype, indicating that the HD-ZIP IIIs are required for GA-induced xylem production (Fig. 3h,i). Taken together, these data show that GA's effect on xylem formation acts via auxin signalling and its downstream factors to define xylem identity.

GA promotes long-distance PAT via PIN1

The PIN auxin efflux carriers play a dominant role in determining how auxin accumulates in different tissues³⁴. Since GA has previously been reported to regulate PIN levels in the root apical meristem^{22,35}, we investigated whether GA also regulates auxin accumulation, and thus auxin signalling, through PIN activity in the vascular cambium. Of the five plasma membrane-localized PINs (PIN1, 2, 3, 4 and 7) (ref. 34), only PIN1-GFP showed consistent expression on the xylem side of the vascular cambium (Extended Data Fig. 4a–e). A detailed analysis revealed that PIN1 has the highest expression in the xylem-side stem cell daughters (position –1), with weaker expression in the neighbouring cells (positions –2 and 1). Following 24 h GA treatment, PIN1 expression spreads towards the phloem to occupy both stem cell daughters (Fig. 4a,d and Extended Data Fig. 5a), thus showing a shift in expression similar to the auxin signalling marker *DR5v2*. (Fig. 3a,c). Unlike in WT, the PIN1 expression in *ga1* is discontinuous around cambium, and this phenotype can be rescued with GA application (Extended Data Fig. 5a). However, the remaining PIN1 expression shows similar radial distribution to WT within the stem cell daughters. GA treatment led to spread of PIN1 expression, as observed in WT (Fig. 4b,d). Since *DR5v2* induction by GA takes longer (48 h) than induction of PIN1 (24 h), we hypothesized that GA-mediated PIN1 upregulation is independent of ARF-mediated auxin signalling. Supporting this hypothesis, GA treatment leads to spread in PIN1 expression in *arf7,19*, similarly to the GA treatment in WT (Fig. 4a,c,d and Extended Data Fig. 5c). Together, these data show that GA promotes PIN1 expression in the stem cells and this is followed by expanded expression of *DR5v2*.

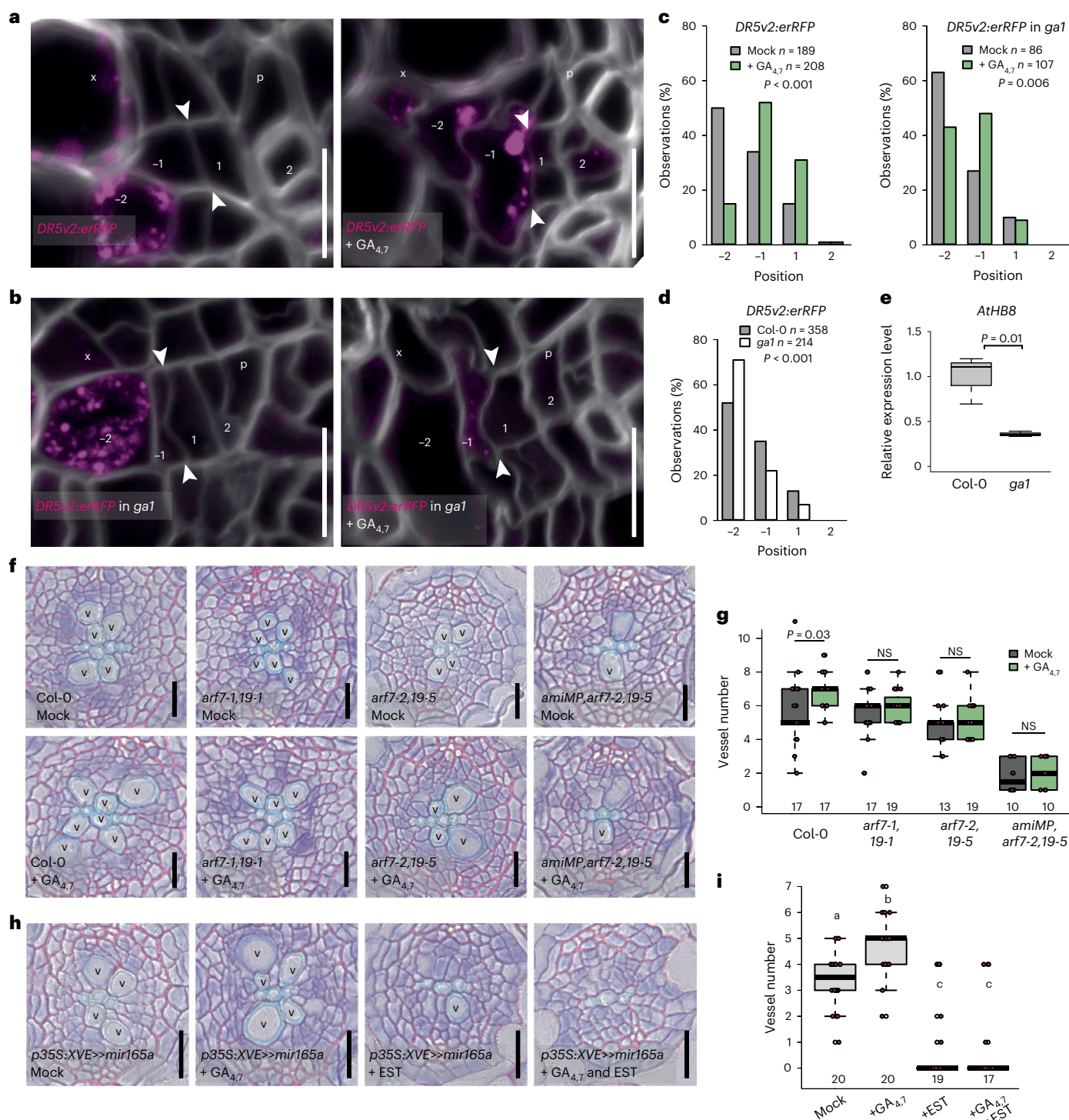


Fig. 3 | Auxin signalling is required for GA to affect xylem development.

a, b, Expression of *DR5v2:erRFP* in the root cambium after a 48 h GA treatment in 14-day-old seedlings of WT Col-0 (**a**) and *ga1* (**b**). White arrowheads indicate the most recent cell divisions. The numbers -2, -1, 1 and 2 indicate the relative position of the cells in respect to the most recent cell division, with negative values towards the xylem and positive towards the phloem. **c**, Counts of the position in the cambium at which the *DR5v2:erRFP* gradient ends. Cellular positions on the x axis correspond with the cellular position in **a** and **b**. **d**, Comparing the *DR5v2:erRFP* gradient in WT and *ga1* backgrounds. **e**, qRT-PCR analysis of the *AtHB8* expression level in WT and *ga1* backgrounds. **f**, Root cross-sections after a 6 day GA treatment in 4-day-old seedlings of Col-0, *arf7,arf19* and *amiMP,arf7,arf19*. **g**, Quantification of the number of secondary xylem vessels in

plants shown in **f, h**. Root cross-sections after a 6 day induction and GA treatment in 4-day-old seedlings of *p35S::XVE>>mir165a*. **i**, Quantification of the number of secondary xylem vessels in plants shown in **g**. Two-tailed chi-square test in **c** and **d**; two-tailed *t*-test in **e**; Kruskal–Wallis test with Bonferroni adjustment in **i**. The boxes in the box-and-whisker plots in **e, g** and **i** show the median and the interquartile range, and the whiskers show the total range. Individual data points are plotted as purple dots. Numbers in **g** and **i** indicate number of samples. Boxes not sharing a lower-case letter in the plots indicate a significant difference, $P < 0.05$. NS, not significant. p, phloem; x, xylem; v, secondary xylem vessels. *n* refers to the total number of observations. Scale bars, 10 μ m (**a** and **b**) and 20 μ m (**f** and **h**). **g** was repeated four times and all other experiments three times.

Previously, PIN1 has been proposed to act both via increased long-distance PAT and via local redirection of auxin fluxes^{11,13,34}. PIN1 has been shown to be basally localized in vascular cells^{11,13,36,37}. Similarly, in the root cambial stem cells, we observed basal PIN1 localization, which did not change after GA treatment (Extended Data Fig. 5b). This suggests that GA does not redirect auxin fluxes within the cambium, implying that long-distance PAT might be affected. To test whether GA enhances long-distance PAT, we performed a PAT assay. Six-day-old seedlings were treated with GA_{4,7} for 1 h, after which seedlings were rinsed and then transferred either directly to discontinuous medium for auxin transport assay or replaced on Murashige and Skoog (MS) medium to grow for an extra 1 or 2 days. For the PAT assay, tritium-labelled indole-3-acetic acid (³H-IAA) was applied to the root–shoot transition zone, and radioactivity was measured in either the upper part of the root (Fig. 4e,f) or the root tip (Extended Data Fig. 6a,b). Increased ³H-IAA signals were observed in the upper part of GA-treated WT roots 1 day after GA application (Fig. 4f). As expected, in the DELLA double mutant *rga.gai*, in which GA signalling is de-repressed³⁸, the ³H-IAA signal did not increase upon GA treatment (Fig. 4f and Extended Data Fig. 6b), thus demonstrating that GA's effect on PAT is caused by the canonical GA signalling pathway. Similarly, *arf7,19* failed to respond to GA (Fig. 4f and Extended Data Fig. 6b), indicating that ARF7/19-mediated auxin signalling is required for GA-induced PAT as well as for xylem formation (Fig. 3f,g).

As GA signalling is able to both enhance PAT and broaden PIN1 expression in the cambium, we postulated that PIN1 might be required for GA's effect on PAT. The *pin1-7* loss-of-function mutant has a lower baseline level of PAT, and *pin1* mutant roots did not show increased ³H-IAA transport upon GA treatment, similar to *rga.gai* and *arf7,19* mutants (Fig. 4f and Extended Data Fig. 6b). However, GA treatment in the triple mutant lacking three of the other plasma membrane-localized PINs, *pin3,4,7*, did result in increased levels of ³H-IAA in roots (Fig. 4f and Extended Data Fig. 6b), indicating that mainly PIN1 is required for GA's effect on long-distance PAT.

In addition to PINs, two ATP Binding Cassette subfamily B (ABC) auxin transporters, ABCB19 and ABCB21, also contribute to maintenance of PAT streams in the vasculature^{39,40}. No change in ABCB19 expression was observed with GA treatment (Extended Data Fig. 7a). However, ABCB21, which is localized almost exclusively to the pericycle⁴⁰, initially increased slightly with GA treatment and maintained over a 24 h period (Extended Data Fig. 7a,b). While rootward auxin transport was severely reduced in *abcb19*, these mutants still showed increased transport with GA treatment (Extended Data Fig. 7c). PAT in *abcb21* was only slightly responsive to GA (Extended Data Fig. 7c). Together these results suggest that GA-enhanced long-distance PAT requires ABCB19 function along with PIN1. Additionally, GA-upregulated ABCB21 probably increases restriction of auxin to the central vasculature, where PIN1 provides directional flux towards the root tip in addition to more localized auxin distributions within vascular cambium.

Since PIN1 has a central role in directional auxin flux along cambium, we next studied whether PIN1 is required for GA to promote secondary xylem production. We first analysed the effect of GA

treatment in two allelic *pin1* mutants, *pin1-1* and *pin1-7*. GA treatment led to an increased number of secondary xylem vessels in WT but not in either of the *pin1* mutants (Fig. 4g,h). In contrast, the *pin3,4,7* mutant responded similarly to WT in terms of xylem production (Fig. 4g,h), indicating a non-redundant function for PIN1 in GA-induced xylem formation. Additionally, *DR5rev:GUS* expression was not induced by GA in the *pin1-7* background (Extended Data Fig. 6c,d). Altogether, our data show that GA promotes broadening of PIN1 expression in the cambium of the hypocotyl and root, which results in increased PAT to and through the root. This leads to a broadening of the enhanced auxin signalling domain in cambium to promote xylem production (Fig. 6a).

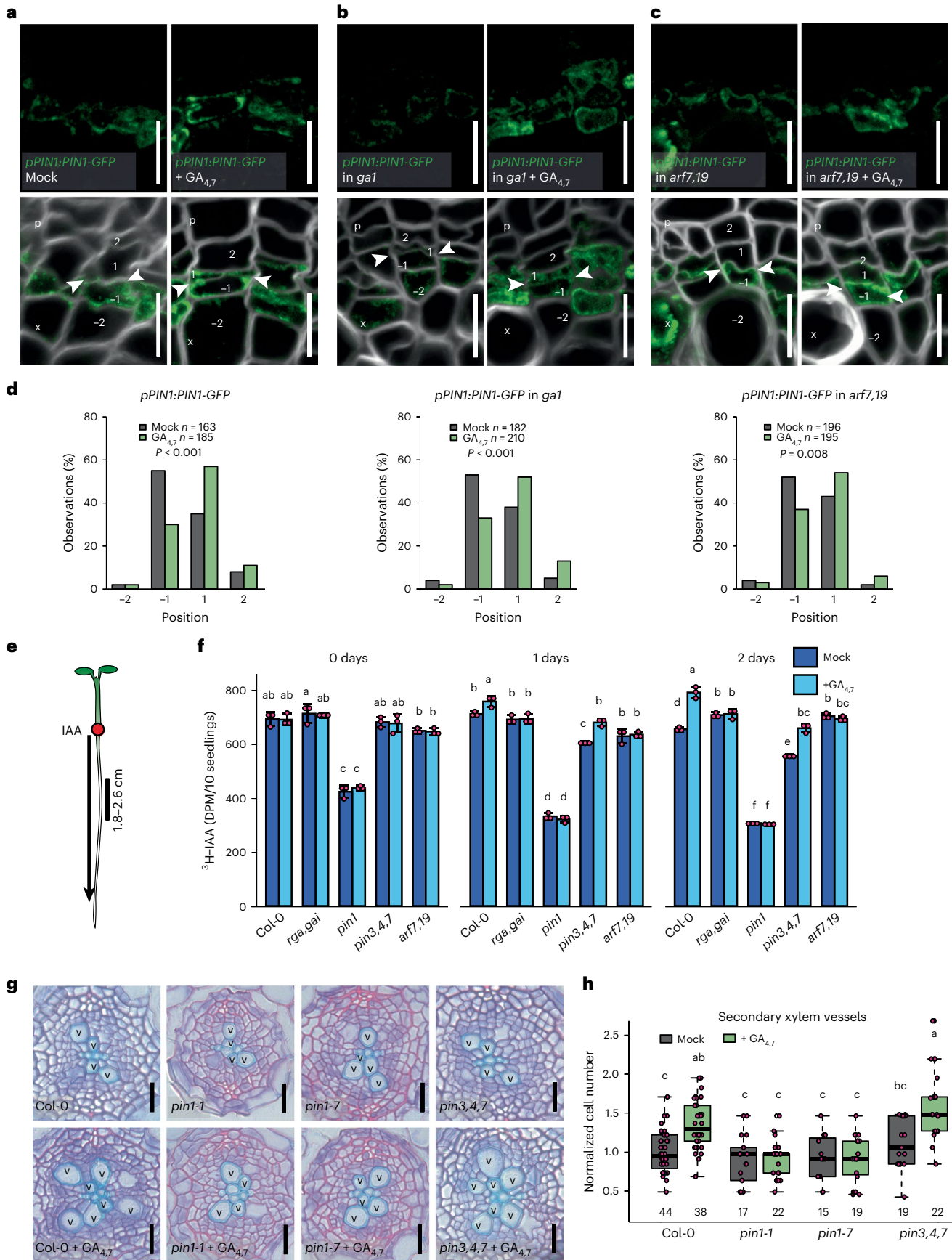
GA treatment occasionally leads to stem cell respecification

Next, we investigated how the GA-induced changes in the width of the auxin maximum alter stem cell fate decisions, shifting from equal xylem and phloem distribution towards favouring xylem production (Fig. 1f–i). First, we investigated the stem cell division dynamics using the stem cell marker *pANT:erRFP* together with labelling dividing cells with 5-ethynyl-2'-deoxyuridine (EdU)⁴¹. *ANT* was typically expressed in both stem cell daughters (mock: 68%; Fig. 5a) and to a lesser degree only in the phloem-side stem cell daughter (32%). After 2 days of EdU tracing, the majority of the EdU-positive cells were in the *ANT* expression domain (mock: 80%; Fig. 5b and Extended Data Fig. 8a). However, following a 2 day GA treatment, a larger proportion of *ANT* expression was restricted to the phloem-side stem cell daughter (GA_{4,7}: 43%; Fig. 5a). In addition, significantly more EdU-positive cells were outside the *ANT* expression domain towards the xylem (mock: 20%; GA: 36%; Fig. 5b and Extended Data Fig. 8b). These data show that GA treatment results in a higher proportion of xylem-side stem cell daughters losing stem cell identity and obtaining xylem identity.

To follow the consequences of altered stem cell dynamics during long-term GA treatment, we carried out a lineage-tracing experiment where single-cell clones marked with GUS expression were induced in the stem cells using the *ANT* promoter (Fig. 5c,d) (ref. 4). After 6 days, under normal growth conditions, stem cell sectors spanned almost equally towards both the xylem and the phloem (Fig. 5e,h), similar to the stem cell sectors generated randomly within the cambium (Fig. 1f,i) and what we have shown earlier⁴. When seedlings are treated with GA, the majority of the stem cell sectors spanned further towards xylem than phloem (Fig. 5f–h). Unexpectedly, a subset of the *ANT* sectors were pushed away from the cambium into the xylem (Fig. 5g, light-blue sectors in Fig. 5h, 21% of the GA sectors), indicating that, occasionally, both stem cell daughters lose their identity and differentiate into xylem after GA application. This led us to hypothesize that when auxin signalling spreads to both stem cell daughters causing them to differentiate into xylem, the adjacent phloem identity cell respecifies as a stem cell. To test this, we performed a lineage-tracing experiment with sectors originating from a single early phloem cell using the promoter of phloem identity gene *PEAR1* (ref. 29) (Fig. 5i,j). Under normal conditions, the active cambium pushes phloem identity cells away from the cambium while they differentiate

Fig. 4 | GA promotes long-distance auxin transport in a PIN1-dependent manner. a–c, Expression of *pPIN1:PIN1-GFP* in the root cambium after a 24 h GA treatment in 14-day-old seedlings of WT (**a**), *gai1* (**b**) and *arf7,19* (**c**). White arrowheads indicate the most recent cell divisions. The numbers –2, –1, 1 and 2 indicate the position of the cells relative to the most recent cell division, with negative values towards the xylem and positive towards the phloem. **d**, Counts of the position in the cambium at which the *pPIN1:PIN1-GFP* gradient ends. Cellular positions on the x-axis correspond with the cellular positions in **a–c**, and *n* refers to the total number of observations. **e**, A schematic explaining the setup of the PAT assay. The red circle indicates the position of ³H-IAA application, and the black arrow shows the direction of IAA movement. The black line indicates the area sampled to detect ³H-IAA. **f**, ³H-IAA transport from the root–shoot transition

zone to 1.8–2.6 cm from the root tip after a 1 h GA treatment in 6-day-old Col-0 and mutant plants. After 0, 1 or 2 days, plants were treated with ³H-IAA for 3 h and then sampled. Data shown are mean ± s.d. (*n* = 3 independent pools of 10). **g**, Root cross-sections after a 6 day GA treatment in 4-day-old seedlings of Col-0 and various *pin* mutants. **h**, Quantification of the number of secondary xylem vessels in plants shown in **f**. Two-tailed chi-square test in **d**; two-way ANOVA with Tukey's post hoc test in **f** and **h**. The boxes in the box and whisker plots show the median and the interquartile range, and the whiskers show the total range. Individual data points are plotted as purple dots. Numbers in **h** indicate number of samples. Boxes or bars not sharing a lower-case letter in the plots indicate a significant difference, *P* < 0.05 Scale bars, 10 μm (**a–c**) and 20 μm (**g**). p, phloem; x, xylem; v, secondary xylem vessel. All experiments were repeated three times.



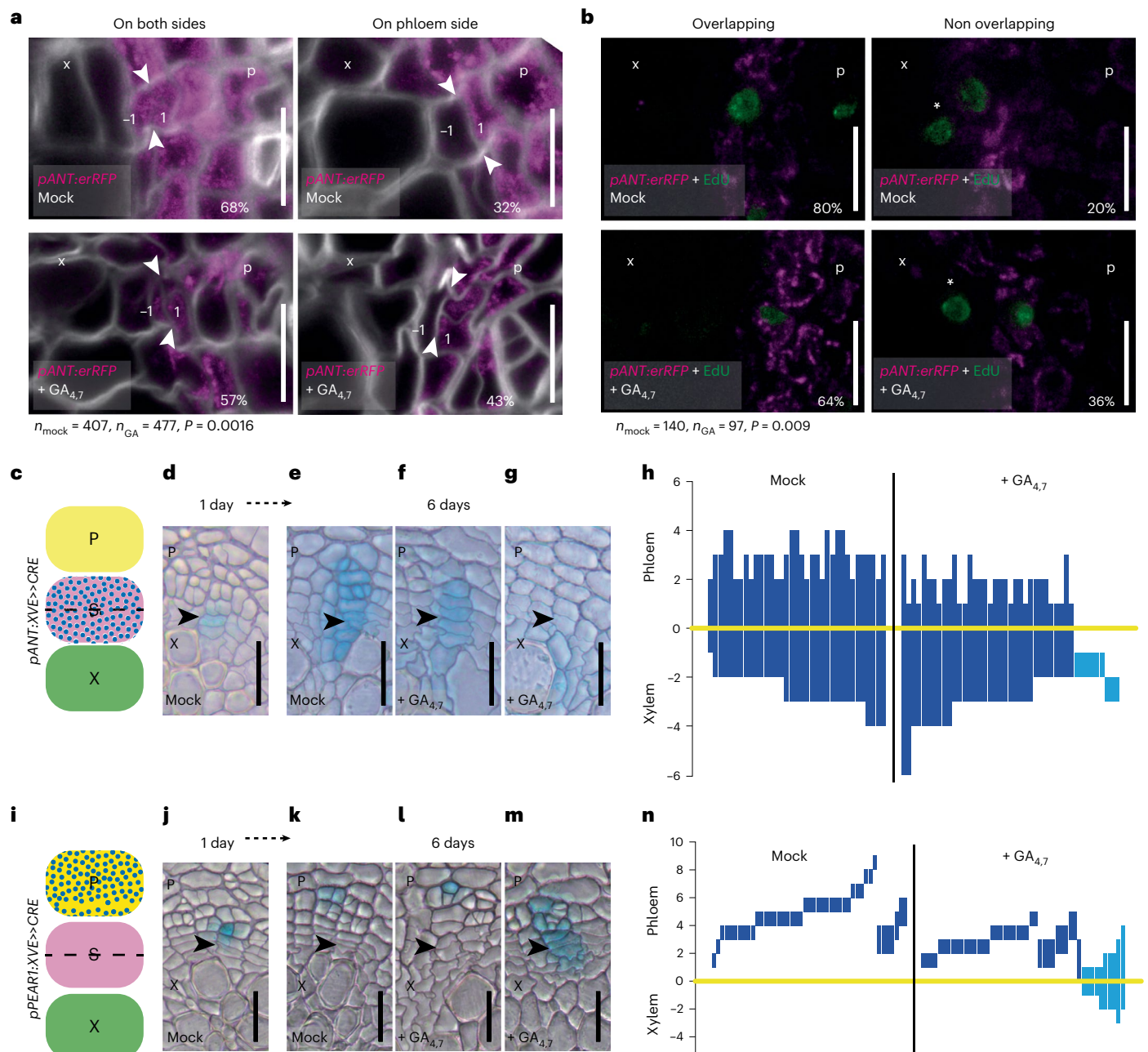


Fig. 5 | GA promotes xylem formation by influencing stem cell dynamics. **a**, Confocal cross-sections of *pANT:erRFP* after a 48 h GA treatment in 14-day-old roots. Expression shift to only on the phloem-side stem cell daughter after GA treatment was significant ($P = 0.0016$). The numbers -1 and 1 indicate the position of the cells relative to the most recent cell division. **b**, Confocal cross-sections of *pANT:erRFP* (magenta) after 6 h of EdU (green) incorporation and 48 h GA treatment in 14-day-old roots. Asterisks indicate EdU-positive cells that do not overlap with *pANT:erRFP* expression. EdU-positive nuclei not overlapping with *ANT* was significantly increased after GA treatment ($P = 0.009$). **c**, A schematic showing where *ANT* sectors originate from within the cambium. **d**, A stem cell sector 1 day after induction in a 14-day-old seedling. **e–g**, A stem cell sector 6 days after induction grown on mock (**e**), a stem cell sector (**f**) and a sector that has lost the stem cell identity (**g**) grown on 2 μM $GA_{4,7}$. **h**, GUS sectors (bars) plotted

based on the position of the thinnest cell wall (yellow line). Note: the light-blue bars highlight the sectors that are only present on the xylem side of the cambium (21% of the GA treated samples). **i**, A schematic showing where the *PEAR1* sectors originate from within the cambium. **j**, A phloem sector 1 day after induction in a 14-day-old plant. **k–m**, A phloem sector 6 days after induction, grown on mock (**k**), a phloem sector (**l**) and a sector containing stem cell (**m**) grown on 2 μM $GA_{4,7}$. **n**, GUS sectors plotted on the basis of the position of the thinnest cell wall (yellow line). Note: the light-blue bars highlight the sectors that have gained stem cell identity (21% of the GA treated samples). x, xylem; p, phloem; S, stem cell. Two-tailed chi-square test in **a** and **b**. Arrowheads in **a**, **e–g**, **k** and **l–m** indicate the most recent cell divisions. Percentages in **a** and **b** indicate frequency of the observed phenotype. Scale bars, 10 μm (**a** and **b**) and 20 μm (**d–g** and **j–m**). All experiments were repeated three times.

into phloem cells, leading to the formation of sectors deep in the phloem (Fig. 5k,n). However, under GA-treated conditions, a subset of phloem lineage sectors is able to produce both xylem and phloem (Fig. 5l–n, light-blue sectors in Fig. 5j, 21% of the GA sectors),

indicating that in these sectors the lineage progenitor reacquired stem cell identity. These data suggest that the original phloem identity cell occasionally respecifies as a stem cell during GA treatment, thus supporting the respecification hypothesis.

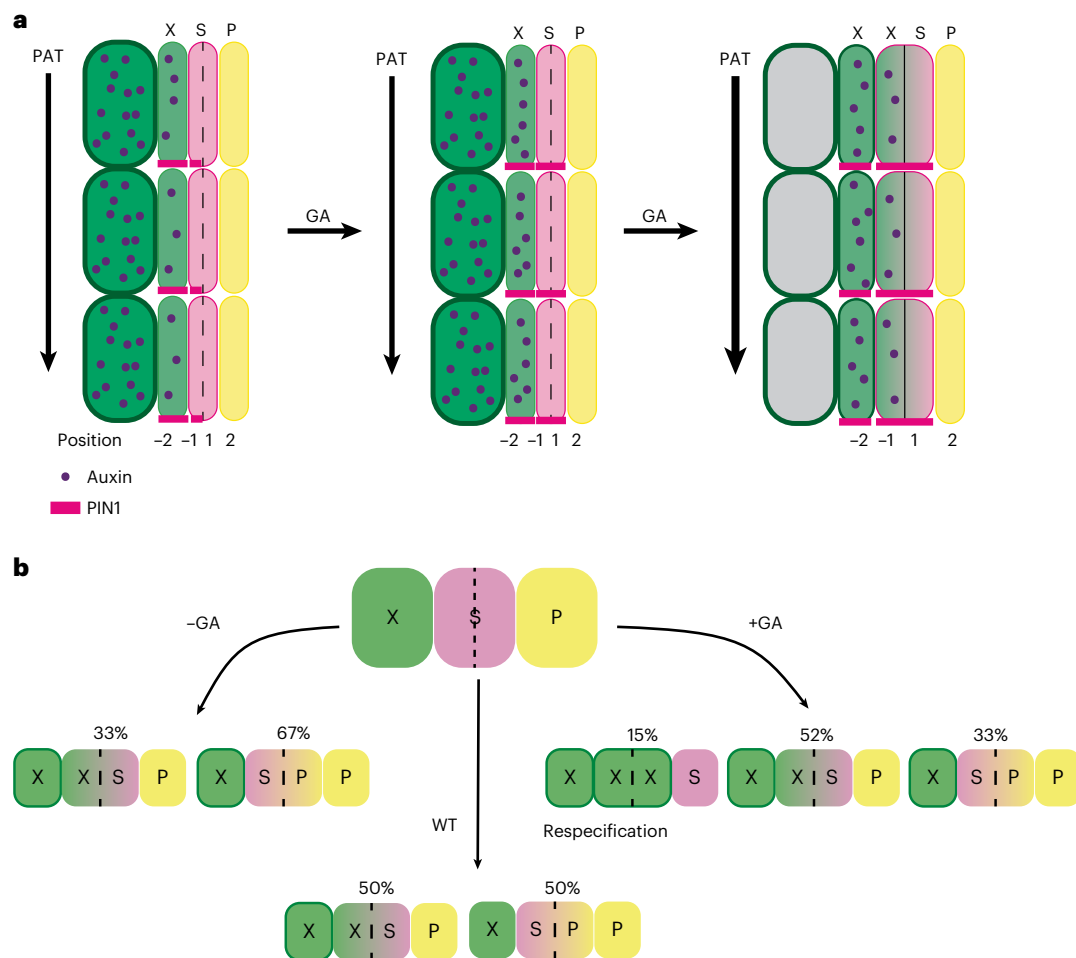


Fig. 6 | Models describing cambium dynamics. a, Model showing the consequences to PIN1, PAT and auxin signalling upon GA treatment. GA induces PIN1 expression in the phloem-side stem cell daughter, leading to increased PAT and widening of the auxin signalling maximum to the xylem-side stem cell daughter, which then gains xylem identity. The numbers -2, -1, 1 and 2 indicate the position of the cells relative to the most recent cell division, with negative values towards the xylem and positive towards the phloem. **b**, Schematic

explaining how the fate of the stem cell daughters is regulated by GA. In normal conditions, cambial stem cells produce an equal amount of xylem and phloem. With low GA levels, stem cell daughters preferentially gain phloem identity, while high GA levels lead to xylem identity, and in extreme cases to the respecification of stem cells from phloem identity cells. Proportions of produced xylem and phloem come from multiple, repetitive, lineage-tracing experiments. X, xylem; S, stem cell (daughters); P, phloem.

Discussion

Previous studies show that elevated GA levels during flowering enhance xylem production in *Arabidopsis* hypocotyls^{17,21} to provide mechanical support for the growing inflorescence stem. Our study shows that GA regulates the balance between xylem and phloem production (Fig. 6) from the onset of secondary growth in the *Arabidopsis* root. Under our experimental conditions, secondary growth in root begins at 4–5 days after sowing, well before the onset of flowering-induced GA production commences. Although the function of GA in early secondary development is poorly characterized, its function as a central integrator of various environmental and endogenous cues⁴² suggests that GA may modulate xylem:phloem ratios in response to environmental conditions.

We show that GA affects xylem proliferation in two ways: first, it increases the number of xylem cells differentiating from the stem cells, and second, it promotes the expansion of secondary xylem vessels, resembling the effect that GA has on other cell types in other tissues⁴³. GA has the opposite effect on phloem production: stem cells produce fewer phloem cells. However, despite the reduced total phloem cell number, a higher proportion of conductive cells are produced. In turn, a GA biosynthesis mutant has a higher proportion of parenchyma cells

than conductive cells. Thus, even though GA levels have a clear impact on phloem parenchyma production, they have a smaller impact on the number of conductive phloem cells. This might be important in ensuring phloem transport capacity regardless of GA status. Auxin promotes primary sieve element differentiation in root tips⁴⁴. Since we show that GA increases auxin signalling in cambium and that GA also promotes conductive phloem formation, we speculate that auxin is needed for the differentiation of conductive phloem cell types also during secondary growth. Supporting this hypothesis, studies have shown that GA and auxin together increase the production of phloem fibres^{45,46}.

We discovered that GA promotes PIN1-dependent and ABCB19/21-assisted PAT, which leads to broadening of auxin signalling in the root cambium during the early stages of secondary development. Previous studies have shown that the DELLAs and ARFs together regulate xylem production in the *Arabidopsis* hypocotyl during flowering²¹. In poplar stems, GA promotes xylem production via *ARF7*, and this is associated with transcriptional upregulation of *PIN1*^{47,48}. During leaf venation, PIN1 promotes auxin accumulation⁴⁹, which leads to activation of ARFs⁵⁰. This in turn promotes *PIN1* expression, thus completing a feed-forward loop⁵¹. Our results show that GA induces PIN1 first, followed by upregulation of the ARF-regulated auxin signalling reporter

DR5v2. This is supported by the finding that PIN1-GFP is induced by GA even in the *arf7,19* mutant background. These results support a mechanism in which GA enters this feed-forward loop by regulating the PIN1 expression pattern, at least during early secondary development in the *Arabidopsis* root.

Organizer cells in meristems position the stem cells to the adjacent cells. In the cambium, organizer cells are defined by a local auxin signalling maximum and subsequent HD-ZIP III expression that leads to cells acquiring xylem identity and cell-autonomous inhibition of cell division⁴. In this study, we show that the position of the maximum regulates the fate decisions of the stem cell daughters. In the presence of high GA and thus elevated PAT, the xylem-side stem cell daughters accumulate high levels of auxin and therefore likely obtain xylem/organizer identity. The phloem-side stem cell daughters retain stem cell identity (Fig. 6a). Occasionally, both daughters accumulate high levels of auxin, leading both to obtain xylem/organizer identity. This forces the neighbouring phloem identity cell to re-specify as a stem cell (Fig. 6b). When GA levels are low, both stem cell daughters have typically low auxin levels, thus making the xylem-side daughter maintain its stem cell identity, since it is located adjacent to an existing auxin signalling maximum. Under these conditions, the phloem-side daughter obtains phloem identity. It is noteworthy that the outcomes described above refer to the most common effects of GA manipulations on auxin maximum and in xylem and phloem production. Moreover, GA manipulations show sizeable variation in the width of PIN1-GFP and *DR5v2* expression (Figs. 3c and 4d). For example, after GA treatment, *DR5v2* expression typically extends to the xylem side daughter. However, there is still a substantial number of cell files where *DR5v2* is expressed deeper in the xylem (Fig. 3c). Indeed, not all cells differentiate as xylem after GA treatment, but 33% of cells differentiate as phloem (Fig. 6b). This variability in the GA regulated stem cell fate decisions probably reflects the GA's role in adjusting, rather than dictating, the ratio of xylem and phloem production.

It is unknown what positions the stem cells adjacent to the auxin maximum. One possibility is that medium auxin levels within the auxin gradient promote stem cell divisions. Supporting this idea, we previously observed an auxin signalling gradient along the cambium using a sensitive auxin signalling reporter⁴. However, it is unclear how such a gradient could robustly position the stem cells. Another possibility is that the auxin maximum initiates a mobile signal, which non-cell-autonomously specifies stem cells in the adjacent position and promotes their division. However, the existence of such a signal remains speculative.

Methods

Plant material and cloning

All entry clones, except *pIR4z-DR5v2*, were generated by PCR amplification of the desired sequence with the primers listed in Supplementary Table 1 followed by recombination into MultiSite Gateway compatible pDONR entry vectors (Supplementary Table 2). The PCR fragment of *DR5v2*, which was amplified from genomic DNA isolated from *DR5v2:nlsGFP*³⁰, was cloned into the *pIR4z-Bsal-ccdB-Bsal* entry vector via Golden Gate cloning to generate *pIR4z-DR5v2*. The construction of *pIR4z-Bsal-ccdB-Bsal* and the Golden Gate cloning were done as previously described⁵². The resulting entry vector, *pIR4z-DR5v2* was assembled together with *p221z-erRFP*⁵³ and *p2R3z-nosT*⁵³ into the destination vector *pHm43GW*⁵⁴ by a MultiSite Gateway LR reaction.

MultiSite Gateway technology was used to combine entry clones carrying a promoter (first box), gene of interest or a tag (second box) and a tag or terminator (third box) with Gateway-compatible binary destination vectors in a MultiSite Gateway LR clonase reaction. All of the expression vectors generated in this study are listed in Supplementary Table 3.

All of the expression vectors were dipped in the Col-0 background, and single insertion lines were screened based on Mendelian

segregation of the selection marker. Several single insertion lines were screened for each construct to observe the most consistent phenotypes or expression patterns. For inducible *RGAA17* lines, five lines with *PEAR* promoter (five out of five behaved as shown), three lines with *ANT* promoter (lines had varying strength, so intermediate one was shown) and eight lines with *AtHBB8* promoter (six out of eight behaved as shown) were analysed. A previously published inducible microRNA (miRNA) against MP (*amiMP*)⁴ line was dipped into the *arf7-2,19-5* background due to silencing issues in the earlier *arf7-1,19-1* background. Seeds published in this study, as well as the already published lines, are listed in Supplementary Table 4. The following transgenic and mutant lines have been reported elsewhere: *pHS:Dbox-CRE x 35S:lox-GUS*⁴, *p35S:XVE>miR165a*⁴, *pANT:XVE-CRE x 35S:lox-GUS*⁴, *pPIN1:PIN1-GFP*⁵⁵, *pPIN1:PIN1-GFP x gal*²², *pPIN2:PIN2-GFP*⁵⁵, *pPIN3:PIN3-GFP*⁵⁶, *pPIN4:PIN4-GFP*⁵⁷, *pPIN7:PIN7-GFP*⁵⁷, *pRGA:GFP-RGA*²⁷, *DR5rev:GUS*⁵⁸, *arf7-1,19-1*⁵⁹, *arf7-2,19-5*⁶⁰, *pin1-7(SALK-047613)*⁶¹, *pin3,4,7*⁶², *pin1-11*, *gal(SALK-109115)*²², *abcb19-101*⁶³ and *abcb21-1*⁶⁰.

Plant growth and chemical treatments

Seeds were surface sterilized first with 20% chlorine and then with 70% ethanol, washed twice with H₂O and then plated on a half-strength growth medium (½ GM, containing 0.5× MS salt mixture with vitamins (Duchefa), 1% sucrose, 0.5 g l⁻¹ 2-(*N*-morpholino)ethanesulfonic acid (MES) pH 5.8 and 0.8% agar) and vernalized at 4 °C for 2 days. In the case of *gal(SALK-109115)*, after sterilization the seeds were soaked in 100 μM GA₃ for 5 days and covered at 4 °C. Before plating, seeds were washed five times with H₂O. The age of the plants was measured from when the plates were vertically positioned in the growth cabinet. The temperature in the cabinets was 22 °C, and they had long-day conditions (16 h of light). To get seeds from *gal* plants, plants growing in soil were sprayed with 100 μM GA₃ twice per week until they had seeds.

Stocks of GA_{4,7} (Duchefa) and GA₃ (Duchefa) (10 mM and 100 mM, respectively) were prepared in 100% EtOH and stored at -20 °C. A 10 mM stock of GA biosynthesis inhibitor paclobutrazol (Sigma) was prepared in 100% EtOH and stored at -20 °C. A 10 mM stock of EdU, a thymidine analogue (Thermo Fisher), was made in dimethyl sulfoxide (DMSO) and stored at -20 °C. A synthetic derivative of oestradiol, 17-*b*-oestradiol (EST) (Sigma), was prepared as a 20 mM stock solution in DMSO and stored at -20 °C.

GA₃ (100 μM) was used for *gal* seed germination and seed production. The working concentration for GA_{4,7} was 2 μM, and paclobutrazol working concentration was 10 μM. XVE-based gene induction was achieved by transferring plants onto plates containing 5 μM 17-*b*-oestradiol or an equal volume of DMSO as a mock treatment. For EdU incorporation, plants were placed in liquid ½GM containing 10 μM EdU for the time stated in each experiment.

GUS staining, microtome sections and histology

The protocol was modified from Idänheimo et al.⁶⁴. Samples were fixed with 90% acetone on ice for 30 min, washed two times with a sodium phosphate buffer (0.05 M, pH 7.2) and then vacuum infiltrated with the GUS-staining solution (0.05 M sodium phosphate buffer, pH 7.2; 1.5 mM ferrocyanide, 1.5 mM ferricyanide, 1 mM X-glucuronic acid and 0.1% Triton X-100). Samples were placed at 37 °C until the staining was at the desired level (the required time varied between different lines).

After staining, the samples were fixed overnight in 1% glutaraldehyde, 4% formaldehyde and 0.05 M sodium phosphate pH 7.2. Fixed samples were dehydrated in an ethanol series (10%, 30%, 50%, 70%, 96% and 2× 100%), with 30 min for each step, and then incubated for 1 h in a 1:1 solution of 100% ethanol and solution A (Leica Historesin Embedding kit). After 2 h in solution A, samples were placed in plastic chambers and filled with 14:1 mixture of solution A: hardener.

Sections of 5 or 10 μm were prepared on a Leica JUNG RM2055 microtome using a microtome knife (Leica Disposable blades TC-65). The sections were imaged without staining or after staining with

Safranin O (Sigma-Aldrich) (1 min in 0.0125% solution, rinsed with water) or double staining with 0.05% ruthenium red (Sigma-Aldrich) and toluidine blue (Sigma-Aldrich) (5 s in each, rinsed between stainings and afterwards with water). Sections were mounted in water and visualized with a Leica 2500 Microscope.

Fluorescent marker analysis: vibratome sections and EdU detection

Using a protocol modified from Smetana et al.⁴, samples were vacuum infiltrated with 4% paraformaldehyde solution (PFA, Sigma) in 1× phosphate-buffered saline (PBS) pH 7.2. After fixation, the samples were washed with PBS and embedded in 4% agarose. Embedded samples were cut with a vibratome into 200 µm sections for confocal analysis. Agarose slices were placed into PBS with SR2200 (1:1000, Renaissance Chemicals) for cell wall staining. For root tip visualizations, we fixed the samples with 4% PFA, cleared them with CLEARSEE and stained the cell walls with SR2200, as in Ursache et al.⁶⁵.

To visualize EdU-positive nuclei, EdU detection was performed on the agarose sections before cell wall staining. The Click-iT EdU Alexa Fluor 488 Imaging Kit (Thermo Fisher) was used for detection with a modified EdU detection mix⁴¹. Samples were incubated in the detection mix for 1 h on ice and then transferred into PBS with SR2200 (1:1000).

Microscopy and image processing

Light microscopy images were taken with a Leica 2500 microscope (20× and 40× objectives). Fluorescent markers were imaged with a Leica Stellaris 8 confocal microscope (63× objective). Confocal images were obtained with Leica Las AF software using PBS or water as the imaging medium. All confocal images with multiple channels were imaged in sequential scan mode. Confocal settings may have varied between experiments but always stayed the same for the experimental sample and the respective control. To better optimize the SR2200 cell wall staining, the signal was sometimes adjusted during imaging and may thus vary between the sample and control.

The Leica Stellaris 8 has a Tau-gating mode that makes it possible to separate GFP signals from background signals. GFP markers were always imaged with this Tau-gating mode, gathering signals between 1.3 ns and 9 ns.

Contrast was adjusted with Adobe Photoshop for the whole GUS images in the following figures: Figs. 1f–h and 5g. A transparent box was added to the figure to make the text more readable in the following figures: Figs. 1a,f–h,j, 2a–d, 3a,b,f,h, 4a–c,g and 5a,b,d–g,j–m and Extended Data Fig. 3a–d,f,g.

Image projections

For image projections (Extended Data Fig. 1f–h), each image was annotated by marking the centre of the root and following the most recent cell division in each cell column in the cambium. The images have been rotated so that the primary xylem axis is oriented in vertical position. Signal data from the image were sampled from the centre point to the edges of the root and aligned to the most recent cell division in the cambial zone. All images in the same treatment were then aligned with the annotated cambial line starting from the centre to the edge. Images within each treatment can therefore be compared and analysed on the basis of the fluorescent signal distribution and intensity, and the location/distance of cambium from the root centre. Image wrapping was done using Python 3.8.10 (ref. 66), and image region of interest (ROI) area extraction was done using several different libraries, including OpenCV2 (ref. 67), Pillow⁶⁸, Matplotlib v2.2.1 (ref. 69) and NumPy⁷⁰. More detailed documentation is available on GitHub (<https://github.com/LMIVainio/PolarUnwrap/find/main>).

Image analysis

Fiji/ImageJ was used for image analysis. When counting secondary xylem vessels, the primary xylem axis was not included and only mature

secondary vessels with light-blue toluidine blue staining were counted. Cells were counted with the cell counter tool. Xylem cells include all the cells inwards of the most recent (thinnest) cell division, so this also sometimes includes the stem cells and stem cell daughters (black line in Fig. 1a). Cells that are not xylem vessels were quantified as xylem parenchyma. Phloem cells were counted as all the cells outwards from the most recent cell division until the periderm border (clearly thicker continuous cell wall on the outskirts of the cross section: red line in Fig. 1a and dashed red line in Extended Data Fig. 1a). Phloem sieve elements were identified by safranin staining, which does not stain these cells, leaving them bright white while other cells show orange staining. In Fig. 4f,g (pin mutants), the data in the graph are combined from four separate experiments, so we normalized the data from the experiments by giving the Col-0 the value of 1 and counting the other values relative to that.

Analysis of the fluorescent markers was done with either Fiji/ImageJ or Leica LAS X lite. For *PIN1* and *DR5*, we quantified the reach of the respective marker expression, meaning the position of the last cell in cambium marker expression was seen. For the spread of *ANT*, we quantified the expression of the *ANT* marker in the cambium, recording whether the marker was expressed on both sides of the most recent cell division or only on the phloem side. Both of these quantifications were carried out only for those radial cell files where the thinnest cell wall was clearly recognizable. For the EdU pulse experiment, we quantified the number of EdU-positive nuclei that either overlapped with the *ANT* signal or were on its xylem side, and the number of those that are only on the xylem side of *ANT* expression.

Auxin transport assays

Six-day-old seedlings on half MS agar plates were treated by applying a thin surface drench of 3 µM GA_{4,7}. After 1 h, the solution was poured off and the seedlings were rinsed and gently blotted to remove excess solution. The seedlings were then either transferred directly to a discontinuous filter paper system for transport assays^{71–73} or allowed to grow for an additional 1–2 days before the assays. For the auxin transport assays, a 200 nl droplet of 10 µM ³H-IAA was placed at the root–shoot transition zone and the seedlings were then incubated under low yellow light. After 3 h, 8 mm segments were collected from two different positions along the root: apex to 0.8 cm (that is, root tip) and 1.8–2.6 cm (that is, upper part). ³H-IAA was measured by liquid scintillation counting. The 1.8–2.6 cm segments contained lateral root primordia and emerged lateral roots. Data shown are mean ± standard deviation (s.d.) (three independent pools of ten seedlings).

qRT-PCR

RNA was collected from 2-cm-long pieces starting just below the hypocotyl of 10-day-old roots where lateral roots had been removed. RNA was isolated using the GeneJET Plant RNA Purification Mini kit (Thermo Fisher) and treated with DNase. Complementary DNA was synthesized from 100 ng of RNA using Maxima H Minus reverse transcriptase (Thermo Fisher) and oligodT primers (Thermo Fisher). The PCR reaction was done on a Bio-Rad CFX384 cyclor using EvaGreen qPCR mix (Solis Biotec) and the following program: 10 min at 95 °C, 50 cycles (10 s at 95 °C, 10 s at 60 °C and 30 s in 72 °C). All of the primers used in qRT-PCR are listed in Supplementary Table 1. The results were normalized, following earlier published methods^{74,75}, to the reference genes *ACT2*, *UBQ10* and *TIP41*. Three biological replicates were used for each line and treatment, as well as three technical replicates.

For ABCB21 expression, 7 day seedlings were surface drenched with MS solution containing solvent control, 1 µM GA or 10 µM GA for 15 min. Solutions were decanted then plates returned upright in light for 24 h. Total RNA was isolated with TRIzol (Thermo Fisher) followed by lithium chloride precipitation. Total RNA (1.5 µg) was reverse transcribed with Superscript III (Thermo Fisher). PCR reactions were performed on a Bio-Rad CFX96 cyclor using SYBR Green master mix

(Applied Biosystems) and the following program: 3 m at 95 °C, 45 cycles (15 s at 95 °C and 1 min at 60 °C). Expression was normalized to the reference genes ACT2 and PP2A. Primers used were from Jenness et al.^{40,76}.

ANT EdU pulse experiment

A short 6 h pulse of 10 µM EdU in liquid ½GM was used, after which the EdU was removed by washing twice for 15 min with liquid ½GM. Washed plants were transferred into 2 µM GA_{4,7} or ethanol (EtOH) plates and allowed to grow for 2 days. After this, they were fixed for agarose sections and confocal analysis.

Lineage tracing

Lineage-tracing experiments were performed in 16- or 14-day-old plants. For the 16-day old *HSdCR* plants, plates were placed at 37 °C for 14 or 17 min. They were then immediately cooled at 4 °C for 15 min (ref. 4). The plants were then transferred to 2 µM GA_{4,7} or EtOH plates for 6 days. For the oestradiol (EST)-inducible lineage-tracing lines, 14-day old plants were incubated in 5 µM EST in liquid ½GM for 2 h (*pPEAR1:XVE>CRE*) or 30 min (*pANT:XVE>CRE*), washed three times for 15 min and then transferred to 2 µM GA_{4,7} or EtOH plates for 6 days. For the *HSdCR* experiments, we considered for the analysis only the sectors that proliferated. Some of the sectors, especially after GA treatment, ended on xylem vessels, which are dead and thus cannot be observed with GUS staining. Therefore, the length of these sectors towards the xylem is an underestimation of the actual length.

General methodology and statistical analysis

The number of individual plants, cross-sections or clones analysed is displayed as *n* in figures or figure legends. The fraction in the corner of some images indicates the frequency of the observation. All statistical analyses were performed using R version 4.1.2 (<http://www.r-project.org/>).

All measurements were taken from distinct samples and the same sample was not measured repeatedly.

Before comparing means, the normality of the data was confirmed with the Shapiro–Wilk test. When doing pairwise comparisons, normally distributed data were analysed with a two-tailed *t*-test and other data with a two-tailed nonparametric Wilcoxon test. When comparing multiple means with each other, a two-way ANOVA with Tukey post hoc was performed. In the case of single variable and not normally distributed data, we used Kruskal–Wallis test with Bonferroni adjustment. Categorical data were analysed with a chi-squared test.

In all of the box plots, the centre line represents the median, and the upper and lower box limits indicate the 75th and 25th percentiles, respectively. Whiskers show the maximum and minimum values, and outliers are shown as circles. Filled circles represent individual data points. In violin plots, the white dot shows the median and the thick line the interquartile range. The thinner line represents the rest of the distribution. Each side of the line is a kernel density estimation that shows the distribution shape of the data. Filled circles represent individual data points.

Softwares used

Leica LAS x, Leica LAS x lite, Bio-Rad CFX Manager, Fiji 1.53, R 4.1.2, R-studio 2022.07.2, Adobe Illustrator, Adobe Photoshop, Python 3.8.10 and MS Office Professional Plus 2016: Excel, Word

Reporting summary

Further information on research design is available in the Nature Portfolio Reporting Summary linked to this article.

Data availability

All data supporting the findings of this article are available in this article and its supplementary information. Source data are provided with this paper. All lines involved in this study are available upon

reasonable request from the corresponding author. Gene accession numbers for genes used in this study: *CYCB1;1*, *AT4G37490*; *PEAR1*, *AT2G37590*; *ANT*, *AT4G37750*; *AtHB8*, *AT4G32880*; *MIR165A*, *AT1G01183*; *MP*, *AT1G19850*; *ARF7*, *AT5G20730*; *ARF19*, *AT1G19220*; *GAI*, *AT4G02780*; *RGA*, *AT2G01570*; *PIN1*, *AT1G73590*; *GAI*, *AT1G14920*; *PIN2*, *AT5G57090*; *PIN3*, *AT1G70940*; *PIN4*, *AT2G01420*; *PIN7*, *AT1G23080*; *APL*, *AT1G79430*; *ABCBI9*, *AT3G28860*; *ABCBI21*, *AT3G62150*. Data for Extended Data Fig. 7a comes from eFP browser http://bar.utoronto.ca/efp2/Arabidopsis/Arabidopsis_eFPBrowser2.html (ref. 77) and Goda et al.^{76,78}.

Code availability

Code used in polar unwrapping and more detailed documentation is available on GitHub (<https://github.com/LMIVainio/PolarUnwrap/find/main>).

References

- Evert, R. *Esau's Plant Anatomy, Meristems, Cells, and Tissues of the Plant Body: Their Structure, Function, and Development*. 3rd edn (John Wiley & Sons, 2006).
- Chaffey, N., Cholewa, E., Regan, S. & Sundberg, B. Secondary xylem development in *Arabidopsis*: a model for wood formation. *Physiol. Plant.* **114**, 594–600 (2002).
- Nieminen, K., Blomster, T., Helariutta, Y. & Mahonen, A. P. Vascular cambium development. *Arabidopsis Book* **13**, e0177 (2015).
- Smetana, O. et al. High levels of auxin signalling define the stem-cell organizer of the vascular cambium. *Nature* **565**, 485–489 (2019).
- Shi, D., Lebovka, I., Lopez-Salmeron, V., Sanchez, P. & Greb, T. Bifacial cambium stem cells generate xylem and phloem during radial plant growth. *Development* **146**, dev171355 (2019).
- Bossinger, G. & Spokevicius, A. V. Sector analysis reveals patterns of cambium differentiation in poplar stems. *J. Exp. Bot.* **69**, 4339–4348 (2018).
- Uggla, C., Moritz, T., Sandberg, G. & Sundberg, B. Auxin as a positional signal in pattern formation in plants. *Proc. Natl Acad. Sci. USA* **93**, 9282–9286 (1996).
- Bagdassarian, K. S., Brown, C. M., Jones, E. T. & Etchells, P. Connections in the cambium, receptors in the ring. *Curr. Opin. Plant Biol.* **57**, 96–103 (2020).
- Brackmann, K. et al. Spatial specificity of auxin responses coordinates wood formation. *Nat. Commun.* **9**, 875 (2018).
- Przemeck, G. K., Mattsson, J., Hardtke, C. S., Sung, Z. R. & Berleth, T. Studies on the role of the *Arabidopsis* gene MONOPTEROS in vascular development and plant cell axialization. *Planta* **200**, 229–237 (1996).
- Galweiler, L. et al. Regulation of polar auxin transport by AtPIN1 in *Arabidopsis* vascular tissue. *Science* **282**, 2226–2230 (1998).
- Verna, C., Ravichandran, S. J., Sawchuk, M. G., Linh, N. M. & Scarpella, E. Coordination of tissue cell polarity by auxin transport and signaling. *eLife* **8**, e51061 (2019).
- Bishopp, A. et al. A mutually inhibitory interaction between auxin and cytokinin specifies vascular pattern in roots. *Curr. Biol.* **21**, 917–926 (2011).
- Rodriguez-Villalon, A. et al. Molecular genetic framework for protophloem formation. *Proc. Natl Acad. Sci. USA* **111**, 11551–11556 (2014).
- Kondo, Y., Fujita, T., Sugiyama, M. & Fukuda, H. A novel system for xylem cell differentiation in *Arabidopsis thaliana*. *Mol. Plant* **8**, 612–621 (2014).
- Mazur, E., Benkova, E. & Friml, J. Vascular cambium regeneration and vessel formation in wounded inflorescence stems of *Arabidopsis*. *Sci. Rep.* **6**, 33754 (2016).
- Ragni, L. et al. Mobile gibberellin directly stimulates *Arabidopsis* hypocotyl xylem expansion. *Plant Cell* **23**, 1322–1336 (2011).

18. Mauriat, M. & Moritz, T. Analyses of GA20ox- and GID1-over-expressing aspen suggest that gibberellins play two distinct roles in wood formation. *Plant J.* **58**, 989–1003 (2009).
19. Israelsson, M., Sundberg, B. & Moritz, T. Tissue-specific localization of gibberellins and expression of gibberellin-biosynthetic and signaling genes in wood-forming tissues in aspen. *Plant J.* **44**, 494–504 (2005).
20. Immanen, J. et al. Cytokinin and auxin display distinct but interconnected distribution and signaling profiles to stimulate cambial activity. *Curr. Biol.* **26**, 1990–1997 (2016).
21. Ben-Targem, M., Ripper, D., Bayer, M. & Ragni, L. Auxin and gibberellin signaling cross-talk promotes hypocotyl xylem expansion and cambium homeostasis. *J. Exp. Bot.* **72**, 3647–3660 (2021).
22. Willige, B. C., Isono, E., Richter, R., Zourelidou, M. & Schwechheimer, C. Gibberellin regulates PIN-FORMED abundance and is required for auxin transport-dependent growth and development in *Arabidopsis thaliana*. *Plant Cell* **23**, 2184–2195 (2011).
23. Sun, T. P. & Kamiya, Y. The *Arabidopsis* GA1 locus encodes the cyclase ent-kaurene synthetase A of gibberellin biosynthesis. *Plant Cell* **6**, 1509–1518 (1994).
24. Bonke, M., Thitamadee, S., Mahonen, A. P., Hauser, M. T. & Helariutta, Y. APL regulates vascular tissue identity in *Arabidopsis*. *Nature* **426**, 181–186 (2003).
25. Bond, J., Donaldson, L., Hill, S. & Hitchcock, K. Safranin fluorescent staining of wood cell walls. *Biotech. Histochem.* **83**, 161–171 (2008).
26. Daviere, J. M. & Achard, P. Gibberellin signaling in plants. *Development* **140**, 1147–1151 (2013).
27. Silverstone, A. L. et al. Repressing a repressor: gibberellin-induced rapid reduction of the RGA protein in *Arabidopsis*. *Plant Cell* **13**, 1555–1566 (2001).
28. Dill, A., Jung, H. S. & Sun, T. P. The DELLA motif is essential for gibberellin-induced degradation of RGA. *Proc. Natl Acad. Sci. USA* **98**, 14162–14167 (2001).
29. Miyashima, S. et al. Mobile PEAR transcription factors integrate positional cues to prime cambial growth. *Nature* **565**, 490–494 (2019).
30. Liao, C. Y. et al. Reporters for sensitive and quantitative measurement of auxin response. *Nat. Methods* **12**, 207–210 (2015).
31. Donner, T. J., Sherr, I. & Scarpella, E. Regulation of preprocambial cell state acquisition by auxin signaling in *Arabidopsis* leaves. *Development* **136**, 3235–3246 (2009).
32. Ursache, R. et al. Tryptophan-dependent auxin biosynthesis is required for HD-ZIP III-mediated xylem patterning. *Development* **141**, 1250–1259 (2014).
33. Mallory, A. C. et al. MicroRNA control of PHABULOSA in leaf development: importance of pairing to the microRNA 5' region. *EMBO J.* **23**, 3356–3364 (2004).
34. Adamowski, M. & Friml, J. PIN-dependent auxin transport: action, regulation, and evolution. *Plant Cell* **27**, 20–32 (2015).
35. Lofke, C. et al. Asymmetric gibberellin signaling regulates vacuolar trafficking of PIN auxin transporters during root gravitropism. *Proc. Natl Acad. Sci. USA* **110**, 3627–3632 (2013).
36. Bennett, T. et al. Connective auxin transport in the shoot facilitates communication between shoot apices. *PLoS Biol.* **14**, e1002446 (2016).
37. Pasternak, T. et al. Protocol: an improved and universal procedure for whole-mount immunolocalization in plants. *Plant Methods* **11**, 50 (2015).
38. Dill, A. & Sun, T. Synergistic derepression of gibberellin signaling by removing RGA and GAI function in *Arabidopsis thaliana*. *Genetics* **159**, 777–785 (2001).
39. Blakeslee, J. J. et al. Interactions among PIN-FORMED and P-glycoprotein auxin transporters in *Arabidopsis*. *Plant Cell* **19**, 131–147 (2007).
40. Jenness, M. K., Carraro, N., Pritchard, C. A. & Murphy, A. S. The *Arabidopsis* ATP-BINDING CASSETTE transporter ABCB21 regulates auxin levels in cotyledons, the root pericycle, and leaves. *Front. Plant Sci.* **10**, 806 (2019).
41. Kotogany, E., Dudits, D., Horvath, G. V. & Ayaydin, F. A rapid and robust assay for detection of S-phase cell cycle progression in plant cells and tissues by using ethynyl deoxyuridine. *Plant Methods* **6**, 5 (2010).
42. Colebrook, E. H., Thomas, S. G., Phillips, A. L. & Hedden, P. The role of gibberellin signalling in plant responses to abiotic stress. *J. Exp. Biol.* **217**, 67–75 (2014).
43. Olszewski, N., Sun, T. P. & Gubler, F. Gibberellin signaling: biosynthesis, catabolism, and response pathways. *Plant Cell* **14**, S61–S80 (2002).
44. Marhava, P. et al. A molecular rheostat adjusts auxin flux to promote root protophloem differentiation. *Nature* **558**, 297–300 (2018).
45. Aloni, R. Role of auxin and gibberellin in differentiation of primary phloem fibers. *Plant Physiol.* **63**, 609–614 (1979).
46. Wang, Y. et al. DELLA–NAC interactions mediate GA signaling to promote secondary cell wall formation in cotton stem. *Front. Plant Sci.* **12**, 655127 (2021).
47. Bjorklund, S., Antti, H., Uddestrand, I., Moritz, T. & Sundberg, B. Cross-talk between gibberellin and auxin in development of populus wood: gibberellin stimulates polar auxin transport and has a common transcriptome with auxin. *Plant J.* **52**, 499–511 (2007).
48. Hu, J. et al. AUXIN RESPONSE FACTOR7 integrates gibberellin and auxin signaling via interactions between DELLA and AUX/IAA proteins to regulate cambial activity in poplar. *Plant Cell* <https://doi.org/10.1093/plcell/koac107> (2022).
49. Verna, C., Sawchuk, M. G., Linh, N. M. & Scarpella, E. Control of vein network topology by auxin transport. *BMC Biol.* **13**, 94 (2015).
50. Powers, S. K. & Strader, L. C. Regulation of auxin transcriptional responses. *Dev. Dyn.* **249**, 483–495 (2020).
51. Wenzel, C. L., Schuetz, M., Yu, Q. & Mattsson, J. Dynamics of MONOPTEROS and PIN-FORMED1 expression during leaf vein pattern formation in *Arabidopsis thaliana*. *Plant J.* **49**, 387–398 (2007).
52. Wang, X. et al. An inducible genome editing system for plants. *Nat. Plants* **6**, 766–772 (2020).
53. Siligato, R. et al. MultiSite Gateway-compatible cell type-specific gene-inducible system for plants. *Plant Physiol.* **170**, 627–641 (2016).
54. Karimi, M., Depicker, A. & Hilson, P. Recombinational cloning with plant gateway vectors. *Plant Physiol.* **145**, 1144–1154 (2007).
55. Xu, J. et al. A molecular framework for plant regeneration. *Science* **311**, 385–388 (2006).
56. Wu, G., Lewis, D. R. & Spalding, E. P. Mutations in *Arabidopsis* multidrug resistance-like ABC transporters separate the roles of acropetal and basipetal auxin transport in lateral root development. *Plant Cell* **19**, 1826–1837 (2007).
57. Blilou, I. et al. The PIN auxin efflux facilitator network controls growth and patterning in *Arabidopsis* roots. *Nature* **433**, 39–44 (2005).
58. Baesso, B. et al. Transcription factors PRE3 and WOX11 are involved in the formation of new lateral roots from secondary growth taproot in *A. thaliana*. *Plant Biol.* **20**, 426–432 (2018).
59. Okushima, Y. et al. Functional genomic analysis of the AUXIN RESPONSE FACTOR gene family members in *Arabidopsis thaliana*: unique and overlapping functions of ARF7 and ARF19. *Plant Cell* **17**, 444–463 (2005).

60. Goh, T., Joi, S., Mimura, T. & Fukaki, H. The establishment of asymmetry in *Arabidopsis* lateral root founder cells is regulated by LBD16/ASL18 and related LBD/ASL proteins. *Development* **139**, 883–893 (2012).
61. Alonso, J. M. et al. Genome-wide insertional mutagenesis of *Arabidopsis thaliana*. *Science* **301**, 653–657 (2003).
62. Govindaraju, P., Verna, C., Zhu, T. & Scarpella, E. Vein patterning by tissue-specific auxin transport. *Development* **147**, dev187666 (2020).
63. Lin, R. & Wang, H. Two homologous ATP-binding cassette transporter proteins, AtMDR1 and AtPGP1, regulate *Arabidopsis* photomorphogenesis and root development by mediating polar auxin transport. *Plant Physiol.* **138**, 949–964 (2005).
64. Idanheimo, N. et al. The *Arabidopsis thaliana* cysteine-rich receptor-like kinases CRK6 and CRK7 protect against apoplastic oxidative stress. *Biochem. Biophys. Res. Commun.* **445**, 457–462 (2014).
65. Ursache, R., Andersen, T. G., Marhavy, P. & Geldner, N. A protocol for combining fluorescent proteins with histological stains for diverse cell wall components. *Plant J.* **93**, 399–412 (2018).
66. Van Rossum, G. a. D., Fred L. *Python 3 Reference Manual* (CreateSpace, 2009).
67. Bradski, G. The OpenCV Library. *Dr. Dobb's Journal of Software Tools* (2000); <http://citebay.com/how-to-cite/opencv/>
68. Clark, A. Pillow (PIL Fork) Documentation. readthedocs. (2015); <https://buildmedia.readthedocs.org/media/pdf/pillow/latest/pillow.pdf>
69. Hunter, J. D. Matplotlib: a 2D graphics environment. *Comput. Sci. Eng.* **9**, 90–95 (2007).
70. Harris, C. R. et al. Array programming with NumPy. *Nature* **585**, 357–362 (2020).
71. Murphy, A., Peer, W. A. & Taiz, L. Regulation of auxin transport by aminopeptidases and endogenous flavonoids. *Planta* **211**, 315–324 (2000).
72. Noh, B., Murphy, A. S. & Spalding, E. P. Multidrug resistance-like genes of *Arabidopsis* required for auxin transport and auxin-mediated development. *Plant Cell* **13**, 2441–2454 (2001).
73. Geisler, M. et al. TWISTED DWARF1, a unique plasma membrane-anchored immunophilin-like protein, interacts with *Arabidopsis* multidrug resistance-like transporters AtPGP1 and AtPGP19. *Mol. Biol. Cell* **14**, 4238–4249 (2003).
74. Livak, K. J. & Schmittgen, T. D. Analysis of relative gene expression data using real-time quantitative PCR and the 2^{(-delta delta C(T))} method. *Methods* **25**, 402–408 (2001).
75. Vandesompele, J. et al. Accurate normalization of real-time quantitative RT-PCR data by geometric averaging of multiple internal control genes. *Genome Biol.* **3**, RESEARCH0034 (2002).
76. Kamimoto, Y. et al. *Arabidopsis* ABCB21 is a facultative auxin importer/exporter regulated by cytoplasmic auxin concentration. *Plant Cell Physiol.* **53**, 2090–2100 (2012).
77. Winter, D. et al. An 'electronic fluorescent pictograph' browser for exploring and analyzing large-scale biological data sets. *PLoS ONE* **2**, e718 (2007).
78. Goda, H. et al. The AtGenExpress hormone and chemical treatment data set: experimental design, data evaluation, model data analysis and data access. *Plant J.* **55**, 526–542 (2008).

Acknowledgements

We thank C. Schwechheimer, E. Scarpella and L. Ragni for providing us published material; and L. Ragni, E. Scarpella, S. el-Showk, H. Iida and X. Zhang for providing feedback on the manuscript. Confocal imaging was performed with help and using equipment of the Light

Microscopy Unit (LMU), University of Helsinki. Special thanks to M. Herpola and M. Iida for helping with daily laboratory related tasks. This work was supported by the Academy of Finland (grant numbers 316544 and 346141 to O.S., L.S., A.S.-G., R.S. and A.P.M.), European Research Council (ERC-CoG CORKtheCAMBIA, agreement 819422 to R.M., B.W., M.L., L.Y., X.W. and A.P.M.), University of Helsinki (HiLIFE fellowship to B.W. and DPPS to R.M. and M.L.) and the US Department of Energy, Basic Energy Sciences, grant no. DE-FG02-06ER15804 to A.S.M. and M.K.J.

Author contributions

A.P.M. conceived the project; A.P.M., R.M. and O.S. designed the experiments; R.M., O.S. and B.W. performed the experiments, except M.K.J. and A.S.M., who designed and conducted the PAT experiment and analysis of ABCBs; L.V. created the APL projections; A.S.-G. provided preliminary data; M.L., L.Y., X.W. and R.S. generated genetic material; A.P.M., R.M. and B.W. wrote the paper with input from all authors.

Funding

Open Access funding provided by University of Helsinki including Helsinki University Central Hospital

Competing interests

The authors declare no competing interests.

Additional information

Extended data is available for this paper at <https://doi.org/10.1038/s41477-023-01360-w>.

Supplementary information The online version contains supplementary material available at <https://doi.org/10.1038/s41477-023-01360-w>.

Correspondence and requests for materials should be addressed to Ari Pekka Mähönen.

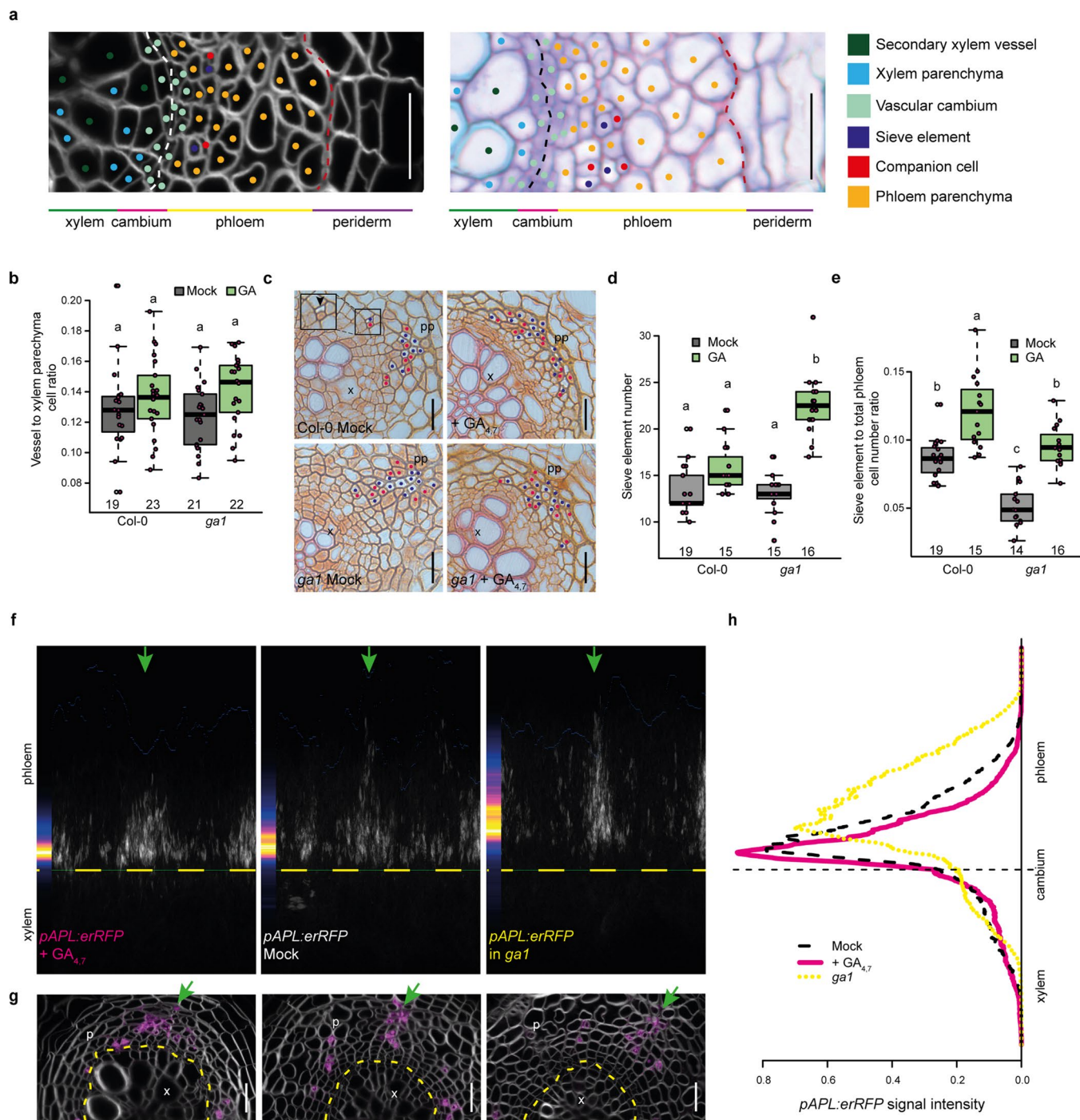
Peer review information *Nature Plants* thanks Yves Deveaux, Yuki Hirakawa and the other, anonymous, reviewer(s) for their contribution to the peer review of this work.

Reprints and permissions information is available at www.nature.com/reprints.

Publisher's note Springer Nature remains neutral with regard to jurisdictional claims in published maps and institutional affiliations.

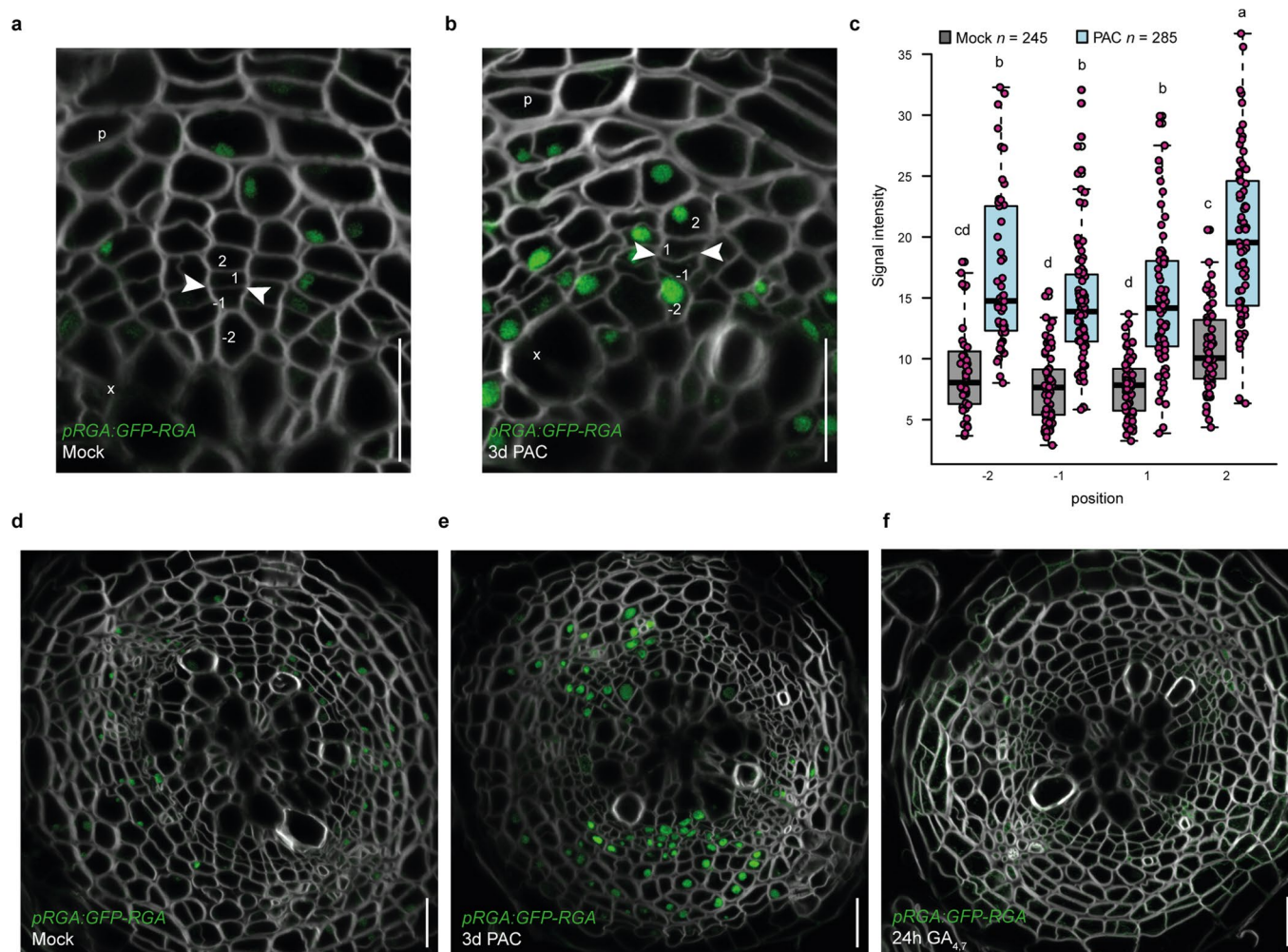
Open Access This article is licensed under a Creative Commons Attribution 4.0 International License, which permits use, sharing, adaptation, distribution and reproduction in any medium or format, as long as you give appropriate credit to the original author(s) and the source, provide a link to the Creative Commons license, and indicate if changes were made. The images or other third party material in this article are included in the article's Creative Commons license, unless indicated otherwise in a credit line to the material. If material is not included in the article's Creative Commons license and your intended use is not permitted by statutory regulation or exceeds the permitted use, you will need to obtain permission directly from the copyright holder. To view a copy of this license, visit <http://creativecommons.org/licenses/by/4.0/>.

© The Author(s) 2023



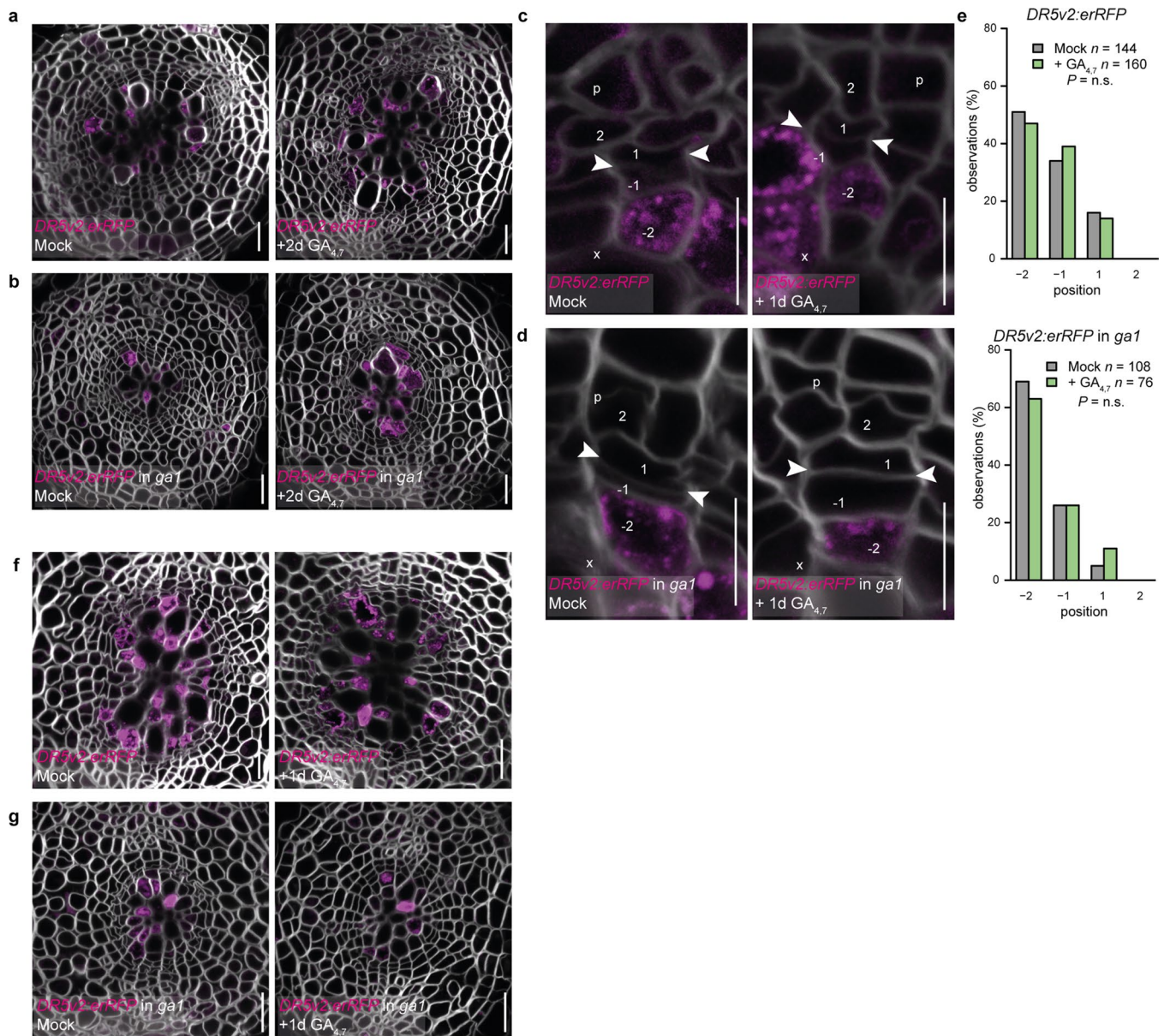
Extended Data Fig. 1 | Characterisation of secondary tissues after GA treatment. **a**, Schematic showing secondary growth tissue and cell types in plastic and agarose sections of 14-day old roots. White/black dotted lines indicate the most recent cell divisions in cambium. Red dotted lines mark the border between the phloem parenchyma cells and the periderm. Different cell types are marked with different coloured dots. **b**, The ratio of secondary xylem vessels to xylem parenchyma cell number from Fig. 1a. **c**, Safranin-stained cross-sections of Col-0 and *ga1*. 4-day old plants treated for 10 days with 2 μ M GA_{4,7} or mock. Safranin O does not stain sieve elements (blue dots), thus they stay white and are easy to distinguish. Neighbouring companion cells are marked with red dots. Zoomed in square shows a non-stained sieve element (black arrowhead). **d**, Quantification of the number of sieve elements in safranin-stained cross-sections. **e**, Ratio of sieve elements to total phloem cell number. **f**, Projections of *pAPL:erRFP* roots of 4-day old plants grown for 10 days on mock or 2 μ M GA_{4,7}

plates or crossed into *ga1*. Each picture is combined from ~15 pictures with the phloem poles and thinnest cell walls aligned. The cambium is marked by a dashed yellow line. Green arrows point to the primary phloem poles. Heat maps on the side show the expression accumulation. **g**, An example of *pAPL:erRFP* expression in 14-day old roots grown with GA_{4,7} or mock or in *ga1* background. The dashed yellow line marks the most recent cell divisions and green arrow points to primary phloem pole. **h**, Graph showing *APL* expression relative to the cambium position. 'x' = xylem, 'pp' = primary phloem pole, 'p' = phloem. Two-way ANOVA with Tukey's post hoc test in **b**, **d** and **e**. The boxes in the box and whisker plots show the median and interquartile range, and the whiskers show the total range. Individual data points are plotted as purple dots. Boxes not sharing a lower-case letter in the plots indicate a significant difference, $P < 0.05$. Scale bars are and 20 μ m (**a**, **c**, **g**). All experiments were repeated three times.



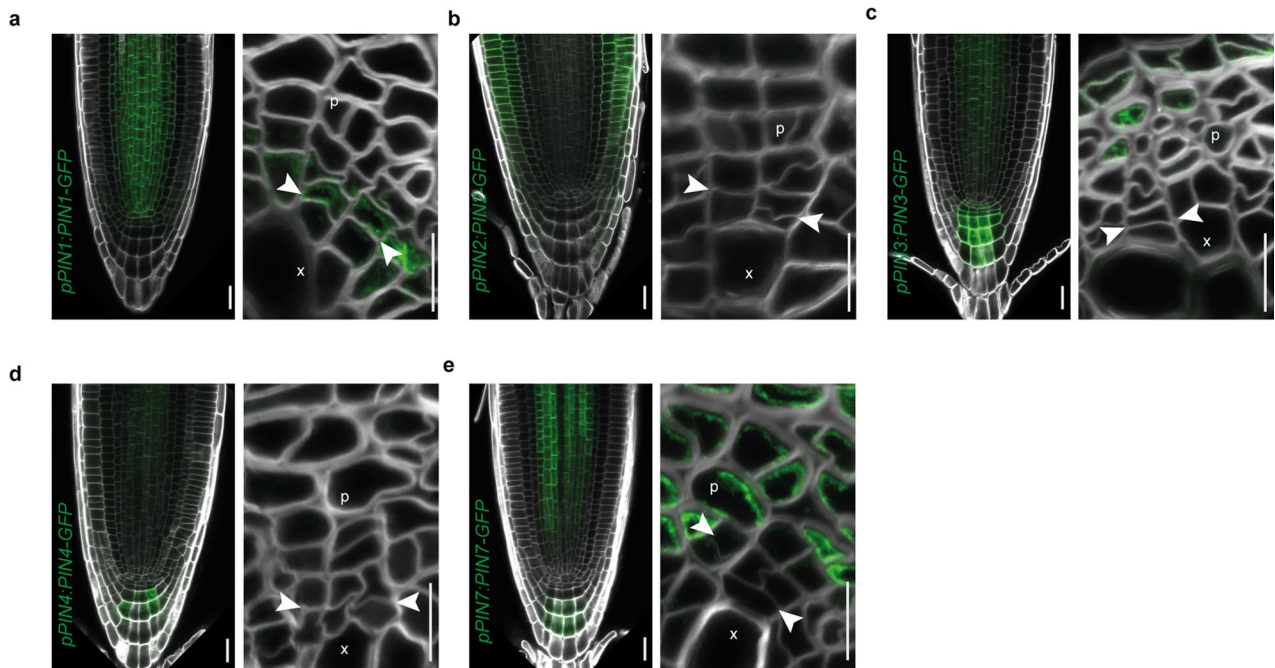
Extended Data Fig. 2 | GA signalling is broadly present during secondary growth. **a**, Expression of *pRGA:GFP-RGA* in 17-days old mock treated root. **b**, RGA expression is increased after 3-days on PAC treatment in 14-days old plants. The numbers ‘-2’, ‘-1’, ‘1’ and ‘2’ indicate the position of the cells relative to the most recent cell division, with negative values towards the xylem and positive values towards the phloem. White arrowheads point to the most recent cell division. **c**, *pRGA:GFP-RGA* signal intensity quantifications from mock and PAC treated roots. **d-f**, Whole cross-sections of 17-day mock treated *pRGA:GFP-RGA*

(**d**); *pRGA:GFP-RGA* after 3-day PAC treatment in 14-days old plants (**e**) and disappeared *pRGA:GFP-RGA* expression after 24 h GA treatment in 14-days old plants (**f**). Scale bars are 20 μm (**a, b, d, e, f**). Two-way ANOVA with Tukey’s post hoc test in **c**. The boxes in the box and whisker plots show the median and interquartile range, and the whiskers show the total range. Individual data points are plotted as purple dots. Boxes not sharing a lower-case letter in the plots indicate a significant difference, $P < 0.05$. ‘x’ = xylem, ‘p’ = phloem.



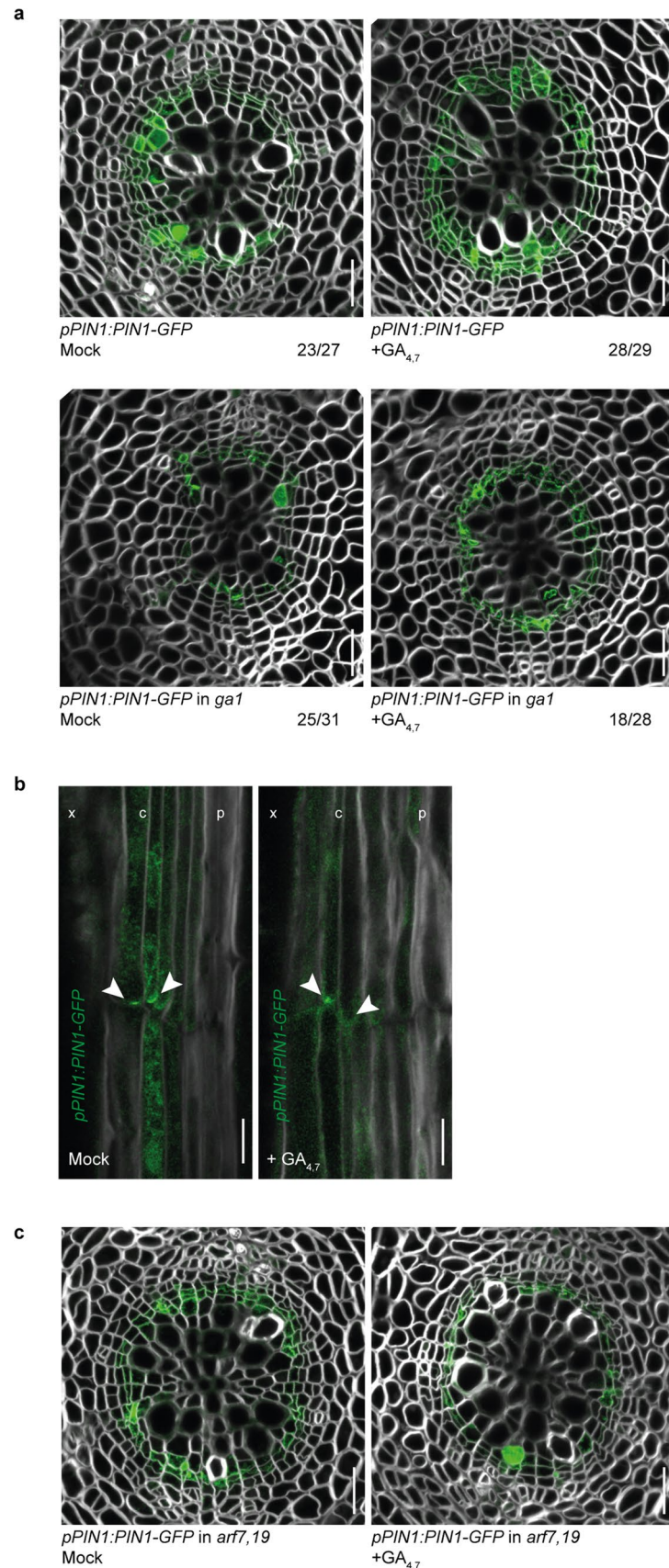
Extended Data Fig. 3 | A 24 h GA treatment is not sufficient to affect auxin signalling in the cambium. **a**, Whole root cross section of *DR5v2:erRFP* in the root cambium after a 48 h GA treatment in 14-day old seedlings of wild type Col-0 (a) and *ga1* (b). **c–d** *DR5v2:erRFP* expression after a 24 h treatment with 2 μ M $GA_{4,7}$ in 14-day old seedlings of wild type Col-0 (c) and *ga1* (d). The numbers ‘-2’, ‘-1’, ‘1’ and ‘2’ indicate the position of the cells relative to the most recent cell division, with negative values towards the xylem and positive towards the phloem.

e, Count of the position in the cambium at which the *DR5v2:erRFP* gradient ends. Cellular positions on the x-axis correspond with the cellular positions in panels c & d. (f–g) Whole root cross section of *DR5v2:erRFP* in the root cambium after a 24 h GA treatment in 14-day old seedlings of Col-0 (f) and *ga1* (g). ‘p’= phloem, ‘x’= xylem, white arrowheads indicate the most recent cell divisions. 2-tailed chi-square test in e. n refers to the total number of observations. Scale bars are 20 μ m (a, b, f, g) and 10 μ m (c, d). All experiments were repeated three times.



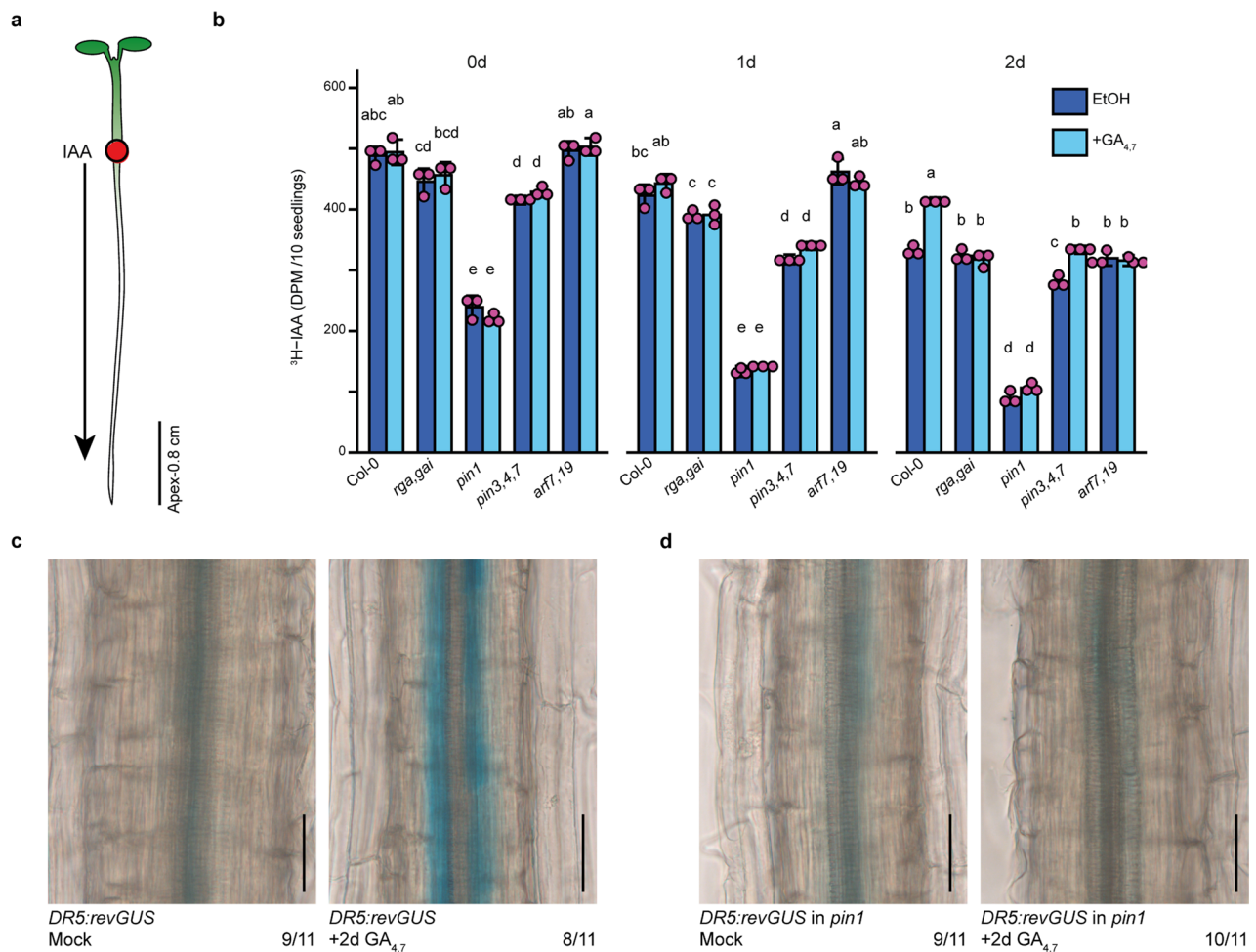
Extended Data Fig. 4 | PIN expression patterns in the root tips and vascular cambium. **a-e**, *pPIN1:PIN1-GFP* (**a**), *pPIN2:PIN2-GFP* (**b**), *pPIN3:PIN3-GFP* (**c**), *pPIN4:PIN4-GFP* (**d**) and *pPIN7:PIN7-GFP* (**e**) expression in 7-day old root tips and 14-day old vascular cambium. Root tips act as positive controls to show that the

marker lines have the expected expression pattern in well-studied parts of the root. 'x' = xylem, 'p' = phloem. Scale bars are 20 μm in the root tips and 10 μm in the cambium. All experiments were repeated three times.



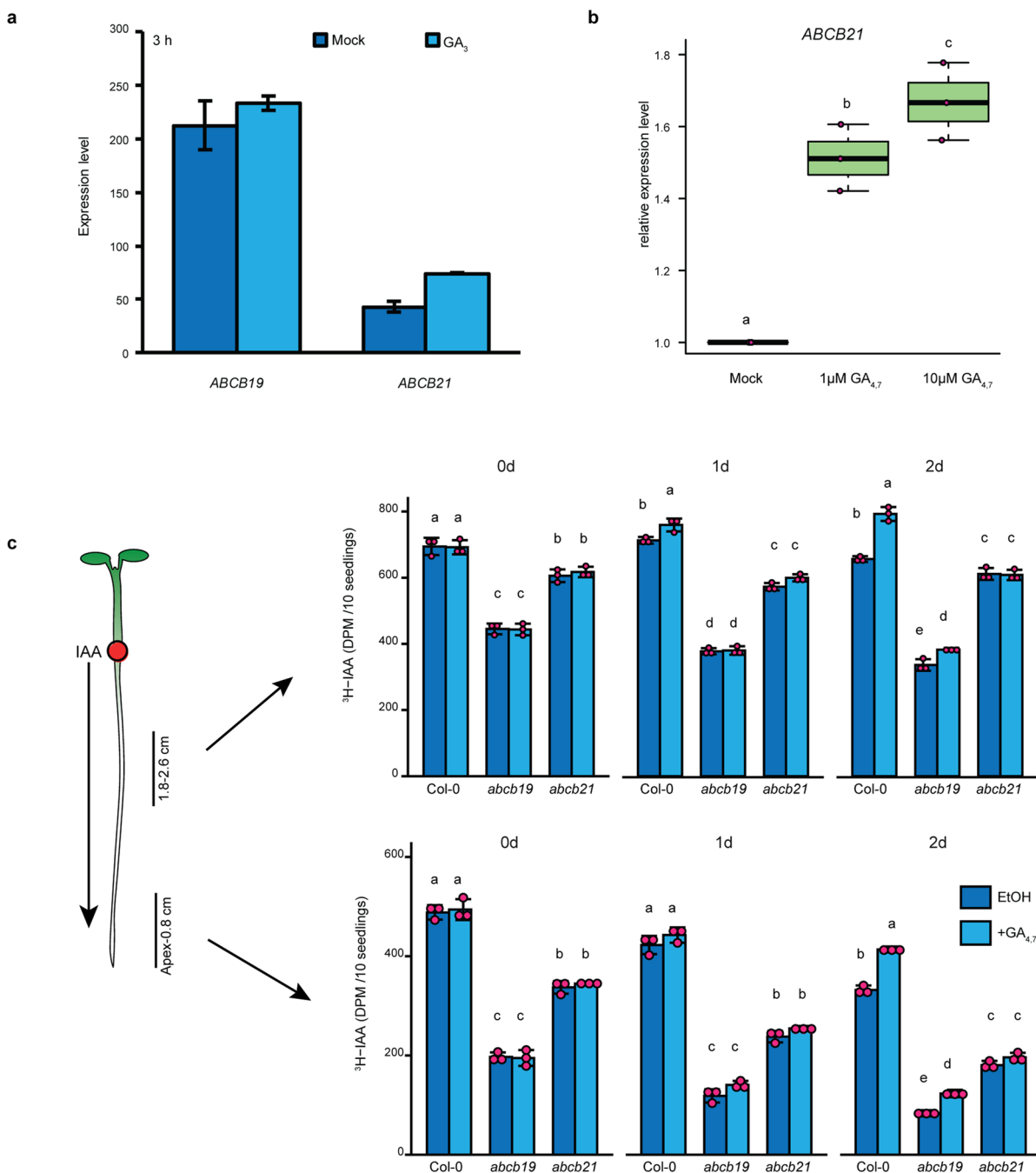
Extended Data Fig. 5 | PIN1 expression in vascular cambium. a, Whole root cross-sections showing *pPIN1:PIN1-GFP* after 24 h GA_{4,7} or mock treatment in 14-day old plants in Col-0 and *ga1* backgrounds. Numbers represent the frequency of the observed phenotypes (continuous or noncontinuous ring of PIN1 expression) in independent roots. **b**, Longitudinal sections showing

pPIN1:PIN1-GFP following a 24 h GA_{4,7} or mock treatment in 14-day old plants. **c**, *pPIN1:PIN1-GFP* expression in *art7,19* mutant after 24 h GA_{4,7} or mock treatment in 14-day old plants. Scale bars are 20 μm (**a,c**) or 10 μm (**b**). 'x' = xylem, 'c' = cambium, 'p' = phloem. White arrowheads in **b** point to cells with PIN1 expression. All experiments were repeated three times.



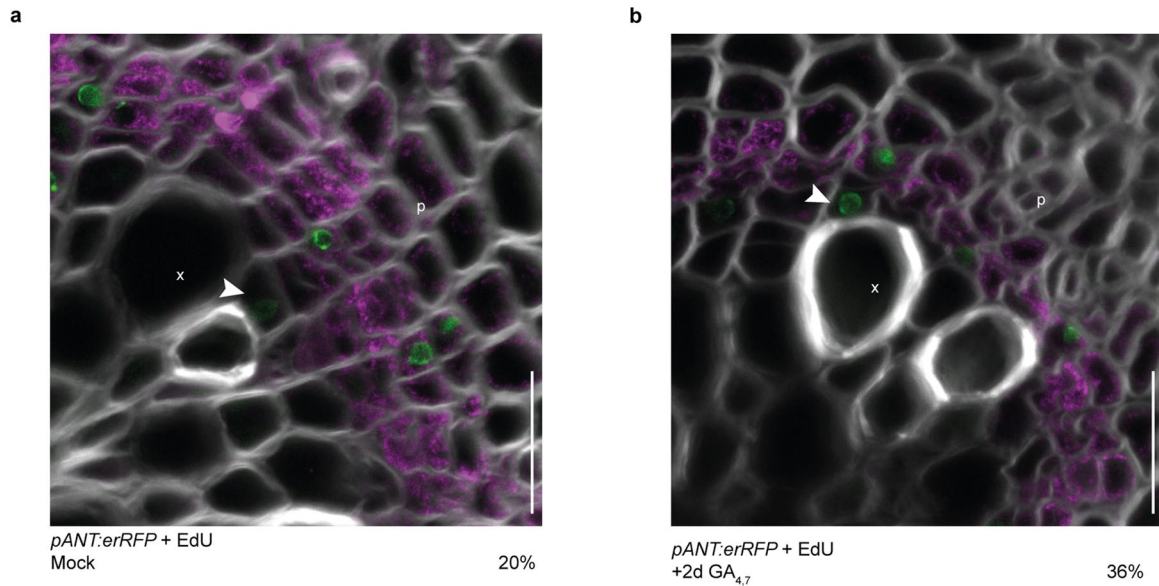
Extended Data Fig. 6 | PAT in root tips. **a**, A schematic explaining the setup of the PAT assay. The red circle indicates the position of ³H-IAA application, black arrow showing the direction of IAA movement. The black line marks the area sampled to detect ³H-IAA. **b**, ³H-IAA transport from the root-shoot transition zone to the root tips after a 1 h GA treatment in 6-day old seedlings of Col-0 and various mutants. After 0, 1, or 2 days, the plants were treated with ³H-IAA for 3 h and then sampled. Data shown are means \pm SD ($n = 3$ independent pools of 10).

Individual data points are plotted as purple dots. **c–d**, Side-view of *DR5rev:GUS* expression after 2-day GA_{4,7} or mock treatment on 8-day old plants in Col-0 (**c**) and *pin1* (**d**) backgrounds. Numbers on the lower right corner are quantifications on how many plants look like the shown example. Scale bars are 50 μ m (**c,d**). Two-way ANOVA with Tukey's post hoc test in **b**. Bars not sharing a lower-case letter in the plots indicate a significant difference, $P < 0.05$.



Extended Data Fig. 7 | PAT in *abcb* mutants. **a**, *ABCB19* and *ABCB21* expression 3 h after treatment with 1 µM GA₃. These data are derived from the Arabidopsis eFP Browser. Data shown are means ± SD. n = 2 microarray experiments. **b**, Quantitative real-time PCR showing *ABCB21* expression 24 h after treatment with 1 or 10 µM GA_{4,7}. Data shown are means ± SD (n = 3 biological replicates, 2 technical replicates). **c**, ³H-IAA transport in *abcb19* and *abcb21* mutant backgrounds from the root-shoot transition zone to 1.8–2.6 mm from the root

tips (upper panels) or to the root tips (lower panels) after 1 h GA treatment (in 6-days old plants). After 0, 1, or 2 days-plants were treated with ³H-IAA for 3 h and then sampled. ³H-IAA transport in Col-0 shown is derived from the same set of experiments shown in Fig. 4 and Extended Data Fig. 4. Figure Data shown are means ± SD (n = 3 independent pools of 10). Individual data points are plotted as purple dots. Two-way ANOVA with Tukey's post hoc test in **c**. Bars not sharing a lower-case letter in the plots indicate a significant difference, *P* < 0.05.



Extended Data Fig. 8 | ANT expression and DNA replication overlap in vascular cambium. a–b, Confocal root cross-sections of *pANT:erRFP* (magenta) after 6 h EdU incorporation (green) and 48 h mock (**a**) or $GA_{4,7}$ (**b**) treatment in 14-days old seedlings. These images are the same as in Fig. 5a, b showing larger area

and the overall expression pattern in the cambium. The percentages in the lower right corners represent the proportion of EdU positive nuclei not overlapping with ANT expression. 'x' = xylem, 'p' = phloem. White arrowheads point to nuclei not overlapping with ANT expression. Scale bars are 20 μ m.

Reporting Summary

Nature Portfolio wishes to improve the reproducibility of the work that we publish. This form provides structure for consistency and transparency in reporting. For further information on Nature Portfolio policies, see our [Editorial Policies](#) and the [Editorial Policy Checklist](#).

Statistics

For all statistical analyses, confirm that the following items are present in the figure legend, table legend, main text, or Methods section.

n/a Confirmed

- The exact sample size (n) for each experimental group/condition, given as a discrete number and unit of measurement
- A statement on whether measurements were taken from distinct samples or whether the same sample was measured repeatedly
- The statistical test(s) used AND whether they are one- or two-sided
Only common tests should be described solely by name; describe more complex techniques in the Methods section.
- A description of all covariates tested
- A description of any assumptions or corrections, such as tests of normality and adjustment for multiple comparisons
- A full description of the statistical parameters including central tendency (e.g. means) or other basic estimates (e.g. regression coefficient) AND variation (e.g. standard deviation) or associated estimates of uncertainty (e.g. confidence intervals)
- For null hypothesis testing, the test statistic (e.g. F , t , r) with confidence intervals, effect sizes, degrees of freedom and P value noted
Give P values as exact values whenever suitable.
- For Bayesian analysis, information on the choice of priors and Markov chain Monte Carlo settings
- For hierarchical and complex designs, identification of the appropriate level for tests and full reporting of outcomes
- Estimates of effect sizes (e.g. Cohen's d , Pearson's r), indicating how they were calculated

Our web collection on [statistics for biologists](#) contains articles on many of the points above.

Software and code

Policy information about [availability of computer code](#)

Data collection

Data analysis

For manuscripts utilizing custom algorithms or software that are central to the research but not yet described in published literature, software must be made available to editors and reviewers. We strongly encourage code deposition in a community repository (e.g. GitHub). See the Nature Portfolio [guidelines for submitting code & software](#) for further information.

Data

Policy information about [availability of data](#)

All manuscripts must include a [data availability statement](#). This statement should provide the following information, where applicable:

- Accession codes, unique identifiers, or web links for publicly available datasets
- A description of any restrictions on data availability
- For clinical datasets or third party data, please ensure that the statement adheres to our [policy](#)

All data supporting the findings of this article are available in this article and its supplementary information. Source data are provided with this paper. All lines involved in this study are available upon reasonable request from the corresponding author.

Gene Accession numbers for Genes used in this study is: CYCB1;1, AT4G37490; PEAR1, AT2G37590; ANT, AT4G37750; AthB8, AT4G32880; MIR165A, AT1G01183;

MP, AT1G19850; ARF7, AT5G20730; ARF19, AT1G19220; GA1, AT4G02780 ; RGA, AT2G01570; PIN1, AT1G73590; GAI, AT1G14920; PIN2, AT5G57090; PIN3, AT1G70940; PIN4, AT2G01420; PIN7, AT1G23080; APL, AT1G79430; ABCB19, AT3G28860; ABCB21, AT3G62150.
Data for Extended data Fig 7a comes from eFP browser "http://bar.utoronto.ca/efp2/Arabidopsis/Arabidopsis_eFPBrowser2.html" (ref 76) and in Goda et. al. 2008 " (ref 77) <https://doi.org/10.1111/j.1365-313X.2008.03510.x>"

Human research participants

Policy information about [studies involving human research participants and Sex and Gender in Research](#).

Reporting on sex and gender	n.a.
Population characteristics	n.a.
Recruitment	n.a.
Ethics oversight	n.a.

Note that full information on the approval of the study protocol must also be provided in the manuscript.

Field-specific reporting

Please select the one below that is the best fit for your research. If you are not sure, read the appropriate sections before making your selection.

Life sciences Behavioural & social sciences Ecological, evolutionary & environmental sciences

For a reference copy of the document with all sections, see nature.com/documents/nr-reporting-summary-flat.pdf

Life sciences study design

All studies must disclose on these points even when the disclosure is negative.

Sample size	No statistic method was used to predetermine the sample size. For all the experiments, we first performed a preliminary analysis with a few samples, and this preliminary analysis was subsequently confirmed with a larger sample size, which was comparable with previous studies (e.g Miyashima et al. 2019 Nature).
Data exclusions	We excluded samples that germinated poorly, or showed overall growth defects that were confirmed genetically not to be related to the genotype. These defects occur occasionally, and are caused by the seed sterilization method used.
Replication	All experiments were repeated at least two times and one representative repeat was shown in the figures.
Randomization	No randomization was applied, but seedlings of different genotypes were grown together in same growth chambers.
Blinding	We did not use blinding. In order to get as objective results as possible, in multiple experiments we had other researchers repeating the experiments.

Reporting for specific materials, systems and methods

We require information from authors about some types of materials, experimental systems and methods used in many studies. Here, indicate whether each material, system or method listed is relevant to your study. If you are not sure if a list item applies to your research, read the appropriate section before selecting a response.

Materials & experimental systems

n/a	Involved in the study
<input checked="" type="checkbox"/>	<input type="checkbox"/> Antibodies
<input checked="" type="checkbox"/>	<input type="checkbox"/> Eukaryotic cell lines
<input checked="" type="checkbox"/>	<input type="checkbox"/> Palaeontology and archaeology
<input checked="" type="checkbox"/>	<input type="checkbox"/> Animals and other organisms
<input checked="" type="checkbox"/>	<input type="checkbox"/> Clinical data
<input checked="" type="checkbox"/>	<input type="checkbox"/> Dual use research of concern

Methods

n/a	Involved in the study
<input checked="" type="checkbox"/>	<input type="checkbox"/> ChIP-seq
<input checked="" type="checkbox"/>	<input type="checkbox"/> Flow cytometry
<input checked="" type="checkbox"/>	<input type="checkbox"/> MRI-based neuroimaging